To the Graduate Council:

I am submitting herewith a thesis written by Melissa Aline Beckmann entitled "Measuring Cell Surface Elasticity on Enteroaggregative *Escherichia coli* 042 Wild Type and Dispersin Mutant by Atomic Force Microscopy." I have examined the final electronic copy of this thesis for form and content and recommend that it be accepted in partial fulfillment of the requirements for the degree of Master of Science, with a major in Life Sciences.

David P. Allison
Major Professor

We have read this thesis
and recommend its
acceptance:

Mitch J. Doktycz

Dabney K. Johnson

Acceptance for the Council:

Anne Mayhew
Vice Chancellor and Dean of
Graduate Studies

(Original signatures are on file with official student records.)

MEASURING CELL SURFACE ELASTICITY ON ENTEROAGGREGATIVE *ESCHERICHIA COLI* 042 WILD TYPE AND DISPERSIN MUTANT BY ATOMIC FORCE MICROSCOPY

A Thesis
Presented for the
Master of Science
Degree
The University of Tennessee, Knoxville

Melissa Aline Beckmann
August 2006

ACKNOWLEDGEMENTS

I am grateful to my major professor, Dr. David P. Allison for giving me support and expert guidance through the nuances of atomic force microscopy. To Claretta Sullivan and all of the members of the Doktycz laboratory who are all fun to work with and provided me with valuable feedback from my data presentations. To Sankar Venkataraman who provided the expertise to analyze the force distance spectroscopy data. To Dr. James P. Nataro who supplied the enteroaggregative *Escherichia coli* 042 strains that made this research possible. To Joe Crabtree at Molecular Imaging Inc. who walked me through the process of thermal noise measurement, automatic spring constant calculations and cantilever sensitivity conversion factors. To the Genome Science and Technology Program that gave me this unique learning experience. To my committee: Dr. Mitch J. Doktycz and Dr. Dabney K. Johnson.

ABSTRACT

Enteroaggregative *Escherichi coli* (EAEC) 042 is a pathogenic strain of *E.coli* that produces a severe diarrhea in humans. A mutant of EAEC 042 that does not produce dispersin, a cell surface protein, is not pathogenic. It has been proposed that dispersin imparts a positive charge to the bacterial cell surface allowing the bacteria to colonize on the negatively charged intestinal mucosa. However, physical properties of the bacterial cell surface, such as rigidity, may be influenced by the presence of dispersin and may contribute to pathogenicity. Using the system developed in our laboratory for mounting and imaging bacterial cells by atomic force microscopy (AFM), in liquid, on gelatin coated mica surfaces, studies were initiated to measure cell surface elasticity of both wild type EAEC 042 that produces dispersin, and the mutant that does not produce dispersin. This was accomplished using AFM force distance (FD) spectroscopy on the wild type and mutant grown in liquid or on solid medium. Images in liquid and in air of both the wild type and mutant grown in liquid and on solid media are presented. This work was done to establish a baseline for future AFM force interaction studies to determine the pathogenic role of the dispersin protein in the wild type bacteria.

TABLE OF CONTENTS

Section/Page

1. INTRODUCTION…….……..……. 1

1.1 Document Layout……..……..……... 1

1.2 Function and Importance of the Gram Negative Cell Envelope…..... 3

1.3 Description of EAEC……..... 5

1.4 Surface Structures and Properties Unique to EAEC 042..... 5

1.5 AFM to Investigate EAEC 042……..……..…….....…. 7

1.6 Significance of Research…….……..……..……. 9

2. ATOMIC FORCE MICROSCOPE……...……..……..…….. 11

2.1 System Description……... 11

2.1.1 Modes of Image Acquisition…..……..…..……..…….. 15

2.1.2 Imaging Environments…….……..... 16

2.1.3 Force Distance Spectroscopy…..……..…… 17

3. MATERIALS AND METHODS……..…….……..…….. 24

3.1 Choice of Mounting Substrate……..…… 24

3.2 Preparation of the Mica Disks for Immobilizing EAEC 042…..…… 24

3.3 Growth of EAEC 042..... 25

3.4 Preparation of EAEC 042 for AFM..……..……..... 25

3.5 Determination of Cantilever Spring Constant……..... 27

3.6. Imaging Environments and Modes of AFM Operation…….…..... 27

3.6.1 Imaging in Air Using Contact Mode……..… 27

3.6.2 Imaging in Water Using Intermittent Contact Mode…….. 28

3.6.3 Force Distance Spectroscopy……. 29

3.7 Analysis of FD Curves……. 30

4. RESULTS AND DISCUSSION……..…..…… 33

4.1 Choice of Mounting Substrate..... 33

4.2 Preparation of the Mica Disks for Immobilizing EAEC 042……..... 33

4.3 Growth and Preparation of EAEC 042 for AFM..... 37

4.4 Determination of Cantilever Spring Constant…….. 38

4.5 Imaging Environments and Modes of AFM Operation……..… 41

4.5.1 Imaging in Air Using Contact Mode…… 42

4.5.2 Imaging in Water Using MAC Mode..……..…… 45

4.6 Force Distance Spectroscopy……. 47

5. CONCLUSIONS AND FUTURE EXPERIMENTS..……..….. 59

LITERATURE CITED…….……..…… 63

APPENDIX…….……..…….…… 73

VITA.…….……..……...…. 75

LIST OF FIGURES

Figure/Page

1. Schematic of a Gram negative bacterium cell envelope…….…….. 3

2. Scanning electron micrographs of 042*pet* (A) and 042*aap* (B)…..…….. 7

3. Scanning electron microscope image of AFM cantilevers……..…… 12

4. Configuration of a piezoceramic tube of an AFM scanner……. 12

5. Schematic of AFM parts and operation…….……... 14

6. AFM deflection detection……..… 14

7. Schematic of a FD curve on a hard surface...…….. 18

8. Raw data FD curves on mica in air and in water……. 20

9. Schematic of a FD curve on a soft surface…….. 21

10. Cantilever deflection on a soft surface…… 22

11. Tip indentation of a soft surface and calculation of the slope ……..... 23

12. Assembly of liquid cell and sample stage…….……. 26

13. Example of a FD curve produced by the gradient analysis method..... 32

14. Contact mode images in air……..... 43

15. Topographic Mac Mode images in water……..... 46

16. Images before and after FD spectroscopy..... 47

17. Raw FD curve made in water on bare mica……... 49

18. Raw FD curve made in water on bare gelatin coated mica……..… 49

19. Raw FD curve made in water on a bacterium…… 50

20. An approach portion of a raw data FD curve on a bacterium ……..... 52

21. The approach portions of experimental FD curves……..…..…….. 53

22. A scanning electron micrograph of 042*pet*……..…….. 61

1. INTRODUCTION

1.1 Document Layout

This thesis describes research conducted to gain an understanding of the pathogenicity of EAEC 042. This first chapter is organized to introduce the background information explaining why cell surface and cell wall elasticities are important and how unique properties of the EAEC 042 are amenable to investigation by AFM. Chapter 2 describes the operation of the AFM and the modes and imaging environments used to visualize surface structures and measure mechanical properties of these bacteria. Chapter 3 describes the materials and methods used in this research. Chapter 4 includes the experimental and analytical challenges of conducting AFM on these bacteria as well as descriptions of how these challenges were overcome during preliminary experiments. Also presented in this chapter are the results from our recent publication, M.A. Beckmann, S. Venkataraman, M.J. Doktycz, J.P. Nataro, C.J. Sullivan, J.L. Morrell-Falvey, D.P. Allison, 2006. Measuring Cell Surface Elasticity on Enteroaggregative *Escherichia coli* Wild Type and Dispersin Mutant by AFM Ultramicroscopy 106: 695-702. The final chapter addresses conclusions that may be drawn from this research and recommends possible directions for future research.

My contributions to the above publication and the research presented in this thesis include literature review, research of topic information, and preliminary experimental investigation. Preliminary data were verified by repeat experiments

conducted and presented in the paper by D.P. Allison.

From this preliminary work, I established that a unique bacteria immobilization technique for AFM imaging previously used in the Allison laboratory is also suitable for sustained FD spectroscopy. In addition, after conducting numerous FD spectroscopy experiments on the EAEC 042 bacteria, I recognized that the standard approach of FD curve analysis was inadequate for determining cell elasticities of these bacteria.

Conventional analysis of bacterial cell elasticity with AFM involves the visual inspection of FD curves which are plots of the force of a probe tip against the distance that the tip indents the bacterium. The slopes of linear areas of these curves have traditionally been used to estimate the rigidity or softness of bacteria cell walls. However, I consistently located more than one linear area per curve which made it difficult to select the slope value that could be used to estimate the whole cell elasticity. I presented these results and analytical difficulties at two different professional meetings. The identification and description of the problem enabled S. Venkataraman to contribute to this work by developing a method of analysis which uses both the FD curve and the raw data file from FD spectroscopy. An algorithm was developed that could be implemented to separate the FD curves into four distinct regions of tip-cell surface interactions while simultaneously producing the slopes of these regions. With this method of analysis, two distinct slopes per FD curve became apparent, one from which the elasticity of the bacteria cell walls was determined and

another from which the elasticity of the outer membrane was determined. The ability to distinctly measure and compare these two different bacteria surfaces could enhance descriptive bacteriology efforts using AFM.

1.2 Function and Importance of the Gram Negative Cell Envelope

In Gram negative bacteria that would include *E. coli*, the structures in contact with the environment make up the cell envelope. Figure 1, a representation of the Gram negative cell envelope showing the thicknesses of its various layers, was adapted from Yao et al., 1999 and Amro et al., 2000.

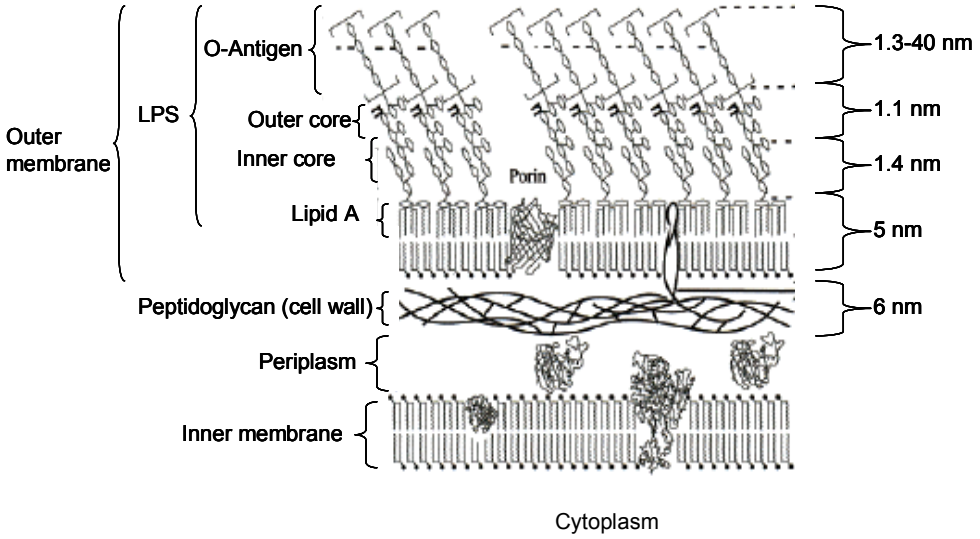


Fig.1. Schematic of a Gram negative bacterium cell envelope.

The most critical of these structures is the stress-bearing cell wall made up of cross-linked peptidoglycan (Yao et al., 1999; 2002). The properties of the cell wall that distinguish it from other cell envelope structures are: it imparts cell shape, maintains internal turgor pressure, acts as a selective barrier to nutrients and metabolites, and allows a bacterium to selectively interact with its environment (Vadillo-Rodriguez et al., 2003). A gel-like periplasm overlies the thin cell wall. The outer-most layer is the lipopolysaccharide (LPS) membrane. The LPS and lipoproteins are covalently attached to the peptidoglycan cell wall (Arnoldi et al., 1998). Approximately 75% of the outer membrane is LPS (3.5 million molecules of LPS) while the remaining 25% is composed of membrane proteins that may be compactly folded and form dense structures that probably represent the stiff regions of the outer membrane (Amro et al., 2000; Schaer-Zammaretti and Ubbink, 2003). Each LPS molecule's length is determined by the number of O-antigen units (2 to 40) at the termini of the LPS molecules (Amro et al., 2000). Longer O-antigens may be bent relative to the membrane normal and lie across other membrane molecules forming a mechanically stable felt-like barrier (Kastowsky et al., 1992). The outer cell membrane may also contain a variety of external structures such as fibrils, fimbriae, pilli, and flagella (Dufrene et al., 2001; Vadillo-Rodriguez et al., 2003).

The combination of all of these structures determines the physicochemical cell surface properties of a particular bacterial strain. These properties, however, are not fixed in space or time but vary with stages of the life cycle (e.g. growth,

division, protection against hostile environments, and host infection) and as a result of mutations (Schar-Zammaretti and Ubbink, 2003; Vadillo-Rodriguez et al., 2003).

1.3 Description of EAEC

EAEC is an emerging diarrheal pathogen that has been associated with endemic and epidemic diarrheal illness both in developing and industrialized countries (Nataro et al., 1998; Sheikh et al., 2002). The pathogenesis of EAEC infection is thought to occur by adherence of the pathogen to the negatively charged intestinal mucosa, most likely of both the small and large intestines, by thin, positively charged, hair-like, adhesive structures called aggregative adherence fimbriae (AAF), followed by a pathological process initiated by one or more enterotoxins (Sheikh et al., 2002; Nishi et al., 2003).

1.4 Surface Structures and Properties Unique to EAEC 042

Working with the pathogenic strain EAEC 042, Nataro's laboratory discovered a novel protein designated Aap (anti-aggregation protein) that is thought to play a significant role in the pathogenic sequence. This 10.2-kDa, low molecular weight protein, is secreted to the exterior environment of the bacteria and appears to form a non-covalently associated capsule on the bacterial cell surface. It is not known whether this capsule is homogenously distributed across the cell surface or whether it is rigid or gel-like in constitution. The positively

charged Aap is believed to cover the negatively charged LPS of the outer membrane. Either the repulsion between Aap and the positively charged AAF fimbriae or the neutralization of the LPS layer by Aap effectively allows the fimbriae to move away from the cell surface. The extended fimbriae can then make contact with the intestinal mucosa and initiate colony formation. In light of this property, Aap has been given the more descriptive name “dispersin” (Nishi et al., 2003). Dispersin is also thought to contribute to pathogenesis by allowing individual progeny of established colonies to swim freely through the mucosa to establish new foci of infection. A mucus penetration assay revealed that a dispersin deletion mutant (042*aap*) was more than an order of magnitude less efficient at penetrating a mucin column than was the wild type parent strain (Sheikh et al., 2002; Nishi et al., 2003).

Several alleles of AAF exist in different strains. The Nataro lab works predominantly with EAEC strain 042 and supplied the wild type and mutant bacteria of this strain for this AFM investigation designed to help characterize the structure and function of the EAEC 042 cell surface. This thesis describes our initial experiments to characterize surface features and their influence on the mechanical dynamics of EAEC 042 strain variants, 042*pet* and 042*aap*. 042*pet* is essentially the wild type bacterium, but carries a mutation in the Pet toxin (plasmid-encoded toxin) to reduce its virulence and danger of infection to lab personnel (Henderson et al., 1999). 042*pet* expresses the AAF and dispersin surface structures when grown in culture broth with at least 0.5% glucose.

042*aap* is a dispersin mutant of the EAEC 042 strain (Sheikh et al., 2002). Like 042*pet*, the dispersin mutant can express AAF, but the fimbriae cannot be extended without the dispersin protein coating as shown in figure 2 (Nishi et al., 2003). We also investigated the effects of two different growth environments, solid agar and broth media, on the cell surface features and dynamics. The bacteria in this figure were cultured in Dulbecco's minimal essential medium with 0.5% glucose overnight. The arrows represent AAF, which splay out from the bacterium in wild type 042, but which typically lie along the bacterial cell surface in 042*aap*. Bars are equal to 1 *μ*m.

1.5 AFM to Investigate EAEC 042

The AFM, invented in 1986, is one of the scanning probe microscope family members (Binnig et al., 1986). There are several specific features of the

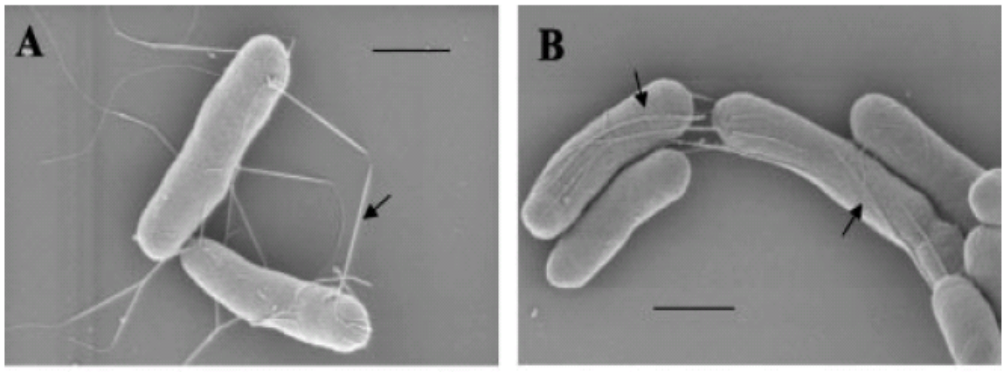


Fig.2. Scanning electron micrographs of 042*pet* (A) and 042*aap* (B).

AFM that have brought it to a leading position in surface science and biological investigations such as descriptive bacteriology. The AFM provides three-dimensional surface topography of cells at nanometer scale resolution by scanning cell surfaces with the tip of a probe mounted at the end of a thin, flexible cantilever.

It is well established that AFM can be used to image living cells under physiological conditions in a nondestructive manner (Schaus and Henderson, 1997). Since AFM images are obtained through physical interaction of a probe tip with the sample, the harsh effects of stains and dyes required for light microscopy and high vacuum and electron beam used in electron microscopy are avoided. Cells can be investigated in a variety of environments (air or liquid) and temperatures while recording real time cellular features and responses *in situ*.

Finally, in addition to imaging, the AFM can also be used to study mechanical, immunochemical, adhesive, and electrostatic properties of cells by measuring the forces of interaction between the probe tip and the cell's surface (Bottomley et al., 1996; Bolshakova et al., 2004). The sensitivity of the AFM cantilever can measure forces at the pico Newton (pN) range, including a force of 16.6 pN, required to rupture a single hydrogen bond (Han et al., 1995). Forces between and within biomolecules have been measured (Allison et al., 2002), and most importantly for this application force measurements have also been made on cell surfaces, including bacterial cell surfaces (Arnoldi et al., 2000; Yao et al., 2002; Dufrene, 2004).

By using the tip to indent cells and the AFM as a force sensor, it has been established that the resulting force curves (plots of force applied versus depth of indentation) provide qualitative measurements of the elastic properties of living cells (Bhushan and Koinkar, 1994; Hoh and Schoenenberger, 1994; Radmacher, 1997; A-Hassan et al., 1998). We investigated the wild type and genetically modified dispersin mutant of the EAEC 042 strain to determine if changes of surface structure mediated by dispersin can be registered by means of AFM. Following these changes should provide valuable insight into the biological importance of dispersin on cellular mechanics and its regulation.

1.6 Significance of Research

A bacterium's cell wall has a critical role in maintaining the overall health of the cell. It is a dynamic structure that continually senses and responds to internal and external cellular environments and makes necessary adjustments to accommodate the cell's needs. Measuring the cell wall elasticity is one way of monitoring these responses. Some of these responses include changing the outer membrane surface structures (e.g. growth of fimbriae and secretion of proteins). Growth of certain structures out of the cell wall and opening of cell wall pores or channels to release proteins can change the elastic properties of the cell wall (Muller and Engel, 1999; Walch et al., 2000). Additionally, these structures may also impart measurable differences in elasticity of the outer membrane.

The design of diagnostic and treatment protocols for EAEC 042 infection is dependent upon knowledge of the functions of its fimbriae and dispersin protein and the surface properties they impart on the cell wall *in vivo*. It has been recognized that important aspects of microbial behavior are controlled by the physicochemical properties of the cell wall (Xu et al., 1996; Dufrene et al., 2001; Vadillo-Rodriguez et al., 2003; Touhami et al., 2003; Schar-Zammaretti and Ubbink, 2003; Bolshakova et al., 2004; Dufrene, 2004). The cell wall is also important in controlling cellular interfacial interactions with the environment, cell-substratum adhesion, and cell-cell aggregation (Touhami et al., 2004). An understanding of the elastic properties of cell surfaces is important since the degree of elasticity will be a function of the combination of the various structural components with one another and reflect complex underlying physiological processes (Vinckier and Semenza, 1998; Haga et al., 2000).

2. ATOMIC FORCE MICROSCOPE

2.1 System Description

The tip of the probe that is used to “feel” and indent sample surfaces to produce images and FD curves is located under the end of a cantilever. Figure 3 is a scanning electron microscope image of commercially available AFM cantilevers showing both V-shaped and beam-shaped cantilevers. A human hair with a diameter of ~100 μm diameter is included as a size reference. The insert shows a higher magnification image showing the probe. The tip of the probe shown has a radius of curvature of ~10 nm (Allison et al., 2002).

The system used in this research is a tip-scanning system in which the cantilever is fastened beneath a scanner and raster scanned across a stationary sample. Scanning is accomplished using a hollow piezoelectric ceramic tube configured to move linearly in X, Y, Z directions. This movement results from mechanical deformation proportional to an applied voltage. Figure 4 shows a hollow piezoceramic tube that is divided into upper and lower portions. The upper portion controls Z plane movement and a lower portion is further divided it into four equal sections for scanning in the X, Y plane. The piezo tube is mounted to the microscope by one end and the cantilever is mounted beneath the free end of the piezo tube. The polarity of the applied voltage determines the direction and extent of the peizo movement by altering the length of the tube, as well as the tube diameter (Müller, 2006; Sensor Technology Limited, 2006).

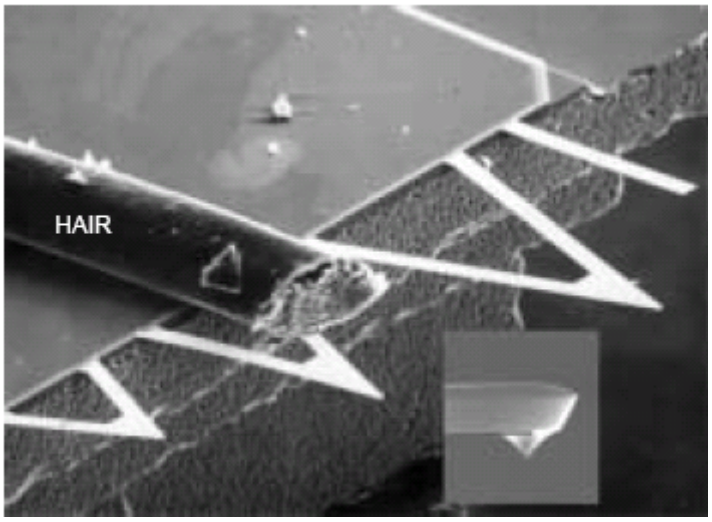


Fig. 3 Scanning electron microscope image of AFM cantilevers.

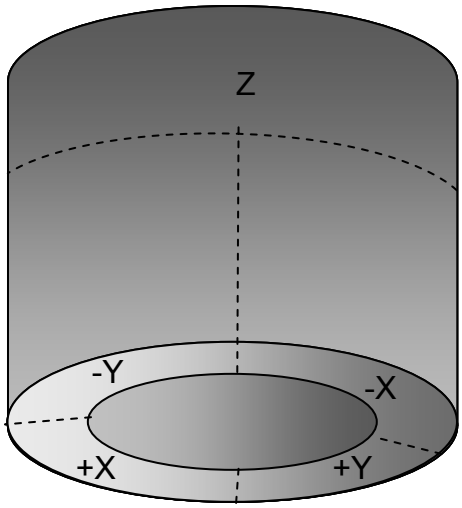


Fig. 4. Configuration of a piezoceramic tube of an AFM scanner.

Raster scanning is a repeated pattern of tip motion from left to right along a line in the X direction followed by an advance of the tip one line in the Y direction. Figure 5 shows the configuration of the scanner relative to the other principle components of the AFM system and their general operation. As the sample surface is raster scanned the cantilever moves up and down (deflects) in response to the surface features. Deflection of the cantilever is monitored by bouncing a laser beam off the back of the cantilever onto a position-sensitive photodetector. Tip-sample interaction distance is controlled by registering the distance that the cantilever deflection deviates from the user defined set-point. This creates an error signal to the controller electronics and a feedback signal in volts is applied to the peizo to move the cantilever up or down in the Z direction to either maintain a constant force on the sample or distance from the sample depending on the mode of operation.

The photodetector measures the vertical cantilever (Z) displacements by the location of the reflected laser spot on the split photodetector relative to (above or below) the user defined deflection set-point as shown in figure 6. The output signals from photodiodes A and B are collected by a differential amplifier. The angular displacement of cantilever results in one photodiode collecting more light than the other photodiode, producing a voltage output signal (the difference between the photodiode signals normalized by their sum) which is proportional to the deflection of the cantilever. The long beam path (several cm) amplifies changes in beam angle so that minute changes in deflection are registered.

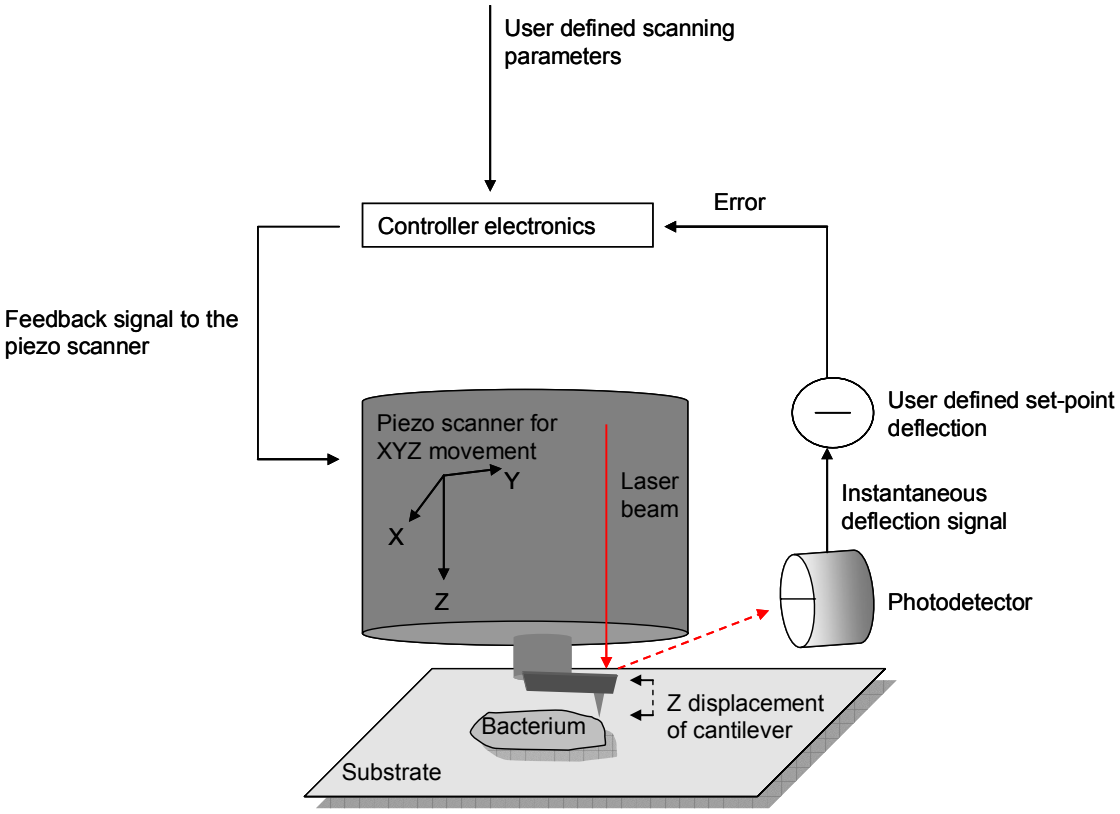


Fig. 5. Schematic of AFM parts and operation.

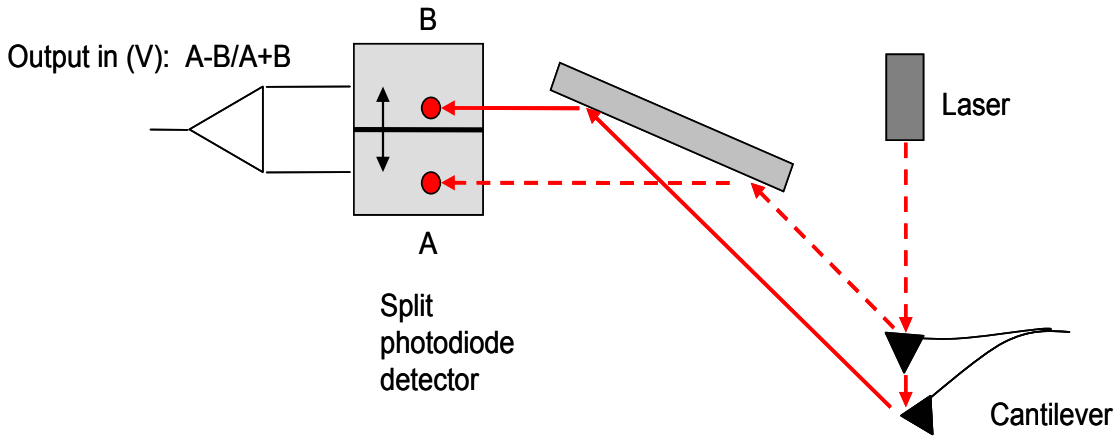


Fig. 6. AFM deflection detection.

The Z position of the tip at each data point in the X-Y plane of the raster scan produces a three dimensional image the surface features. The number of voltage points collected along each X, Y scan line is user-defined in increments of 256. The vertical (Z) resolution achievable is on the Angstrom level and the lateral (X, Y) resolution is on the sub-nanometer level with a probe such as the one shown in figure 3.

2.1.1 Modes of Image Acquisition

There are a number of AFM operating modes that can be used to image various surfaces. The two modes used in this research were contact mode and intermittent contact mode.

In the contact mode, the tip is forced against and dragged across the sample surface during the raster scan. The feedback control loop maintains the force on the sample while the tip is scanned across the surface so that vertical movement of the tip follows the surface profile and is recorded as the surface topography by the AFM.

The type of intermittent contact mode used was the MAC Mode (magnetic alternating current). MAC Mode requires the use of a cantilever that has a magnetic coating applied to its back side that causes the cantilever to vertically oscillate at its resonant frequency above the sample surface when an external alternating magnetic field is applied (Han et al., 1996). The tip alternately oscillates at a high frequency above the surface then approaches the surface to

near-contact where the frequency of oscillation dampens. At near-contact the cantilever oscillation is reduced due to energy loss caused by the tip's proximity to the surface. The oscillation amplitude is maintained throughout the scanning process by the feedback system as the tip follows the topography of the sample surface (Molecular Imaging Inc., 2006).

The mode of operation is critical to the appearance of cells and their surfaces. In general the contact mode provides higher resolution imaging of minor surface details than the intermittent contact mode. A drawback in using the contact mode is the tip is subject to permanent damage or accumulation of debris from its contact with surfaces. Additionally, the contact force can also damage or change the natural conformation of the cell surfaces or dislodge the sample from the surface. MAC Mode intermittent contact operation applies a small amount of pressure to the sample, but not as much as contact mode and is less likely to alter the natural height of cells or damage the tip. Therefore, topographical images obtained in the MAC Mode are more representative of cell dimensions than contact mode images because the tip does not continuously press down on the cells. The MAC Mode is also less likely to dislodge the bacteria.

2.1.2 Imaging Environments

The imaging environment is also critical to the appearance of biological surfaces and each sample requires a unique approach. Successful imaging of Gram-negative bacteria is a challenge due to the dynamics of the cellular

filaments and LPS carbohydrate chains described in Chapter 1 (Bolshakova et al., 2001). Imaging in air and water environments allows different morphological features of interest to be investigated. When dry bacteria are imaged in air, the cell dimensions are distorted by dehydration but the extracellular structures collapse on the cell surface and allow small surface details and ultrastructures such as flagella to be imaged with high resolution. Since bacteria normally live in aqueous environments, liquid imaging results in more accurate measurements necessary for comparison of cells' natural dimensions and dynamics. When imaged in liquid, the normal, overall dimensions of cells (height, width and length) can be observed, but hydration leads to mobility of the extracellular structures which decreases the imaging resolution of surface details (Bolshakova et al., 2001).

2.1.3 Force Distance Spectroscopy

The AFM can be used to study the mechanical property of an entire sample surface (force mapping) or a single X, Y point on the sample surface through the measurement of FD spectroscopy curves. To measure at single points, in the contact mode the X, Y scan size is set to zero and the cantilever tip is positioned on the scanned image on the computer screen by cursor placement. The scanner is lowered in the Z direction applying a force against the surface with the tip. This produces a FD curve, a plot of the vertical force (recorded in volts) that the tip applies to the surface against the Z position of the

scanner as it is ramped toward the sample. The vertical force (F_{sum}) acting normally between the tip and the sample is proportional to the distance of deflection of the cantilever according to Hooke's law $F_{sum} = k_c \Delta z$, where the distance of the vertical deflection is Δz and k_c is the cantilever spring constant.

To determine the distance of the vertical deflection the distance that the cantilever actually deflects for a certain measured change in photodetector voltage must be determined. This value depends on the type of cantilever and the optical path of the detection laser, and will be slightly different each time the cantilever is mounted in the instrument (JPK Instruments, 2006). The cantilever deflection is calibrated by conducting a FD curve on a hard reference surface, usually the surface that the sample is mounted on. The conversion factor is determined as illustrated in figure 7.

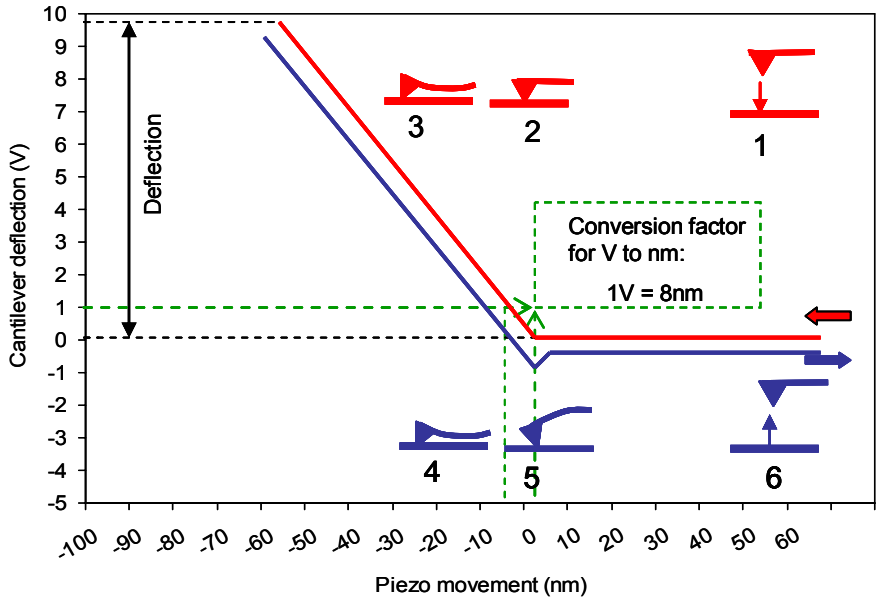


Fig. 7. Schematic of a FD curve on a hard surface.

Figure 7 is a schematic of a FD curve showing the sequence of cantilever movements during the cycle of a FD measurement on a hard reference surface. In this figure, the cantilever, with a spring constant of 0.10 nN/nm, acts as a single spring being compressed as its tip is pressed against a hard surface without indenting the surface. The distance of compression is measured as deflection on the Y axis. The piezo scanner moves the cantilever to the surface in the Z direction. The distance that the piezo advances is measured on the X axis.

The red and blue colors of the curve and cantilevers represent the cantilever approach and retraction portions of the complete cycle respectively. At the right side of the curve, the piezo scanner is well above the surface and approaching the surface in the Z direction. The distance that the piezo advances is measured on the X axis. The cantilever is not deflected since the tip is not touching the surface (position 1). As the scanner progresses downward toward the surface, attractive forces bring the tip and surface into contact (position 2). As the scanner continues downward, the cantilever deflects away from the surface due to repulsive forces (position 3). The gradient of the repulsive contact region (between positions 2 and 3) is marked with green dotted lines and is used to determine the conversion factor. In this case the conversion factor is 8 nm per V. At the end of the user defined Z range, the scanner begins to retract and pulls the tip away from the surface. The cantilever deflection retraces the same curve down to position 5 where a thin layer of water present on many surfaces in air exerts an attractive capillary force and holds the tip in contact with the surface as

the scanner retracts. This causes the cantilever to deflect toward the surface (position 5). As the scanner continues to retract, the capillary force is broken and the cantilever returns to its original undeflected status (position 6) (A-Hassan et al., 1998). This is illustrated in an actual “raw” data FD curve conducted on bare mica in figure 8, when FD spectroscopy is performed in air (curve on left), the capillary forces are large (blue line) when FD spectroscopy is performed in water (curve on right), the capillary force is isotropic and the retract portion of the curve traces the approach portion more closely from beginning to end.

Figure 9 is a schematic of a FD curve showing the sequence of the cantilever’s movements during the cycle of a FD measurement on a softer surface such as that of a bacterium (gray rods). Only the approach portions of FD curves are used in elasticity measurements, so only this portion is shown in this schematic. In figure 9, at position 3 the tip indents the surface.

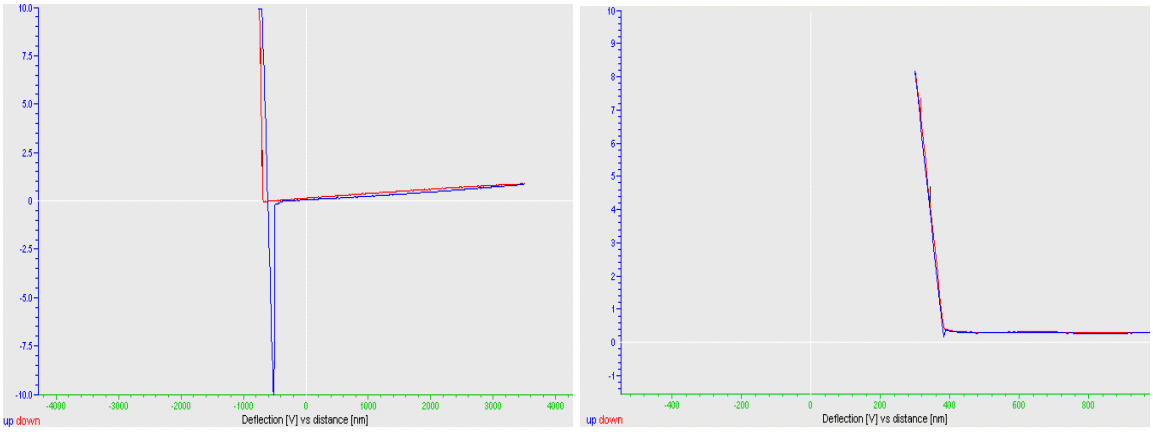


Fig. 8. Raw data FD curves on mica in air and in water.

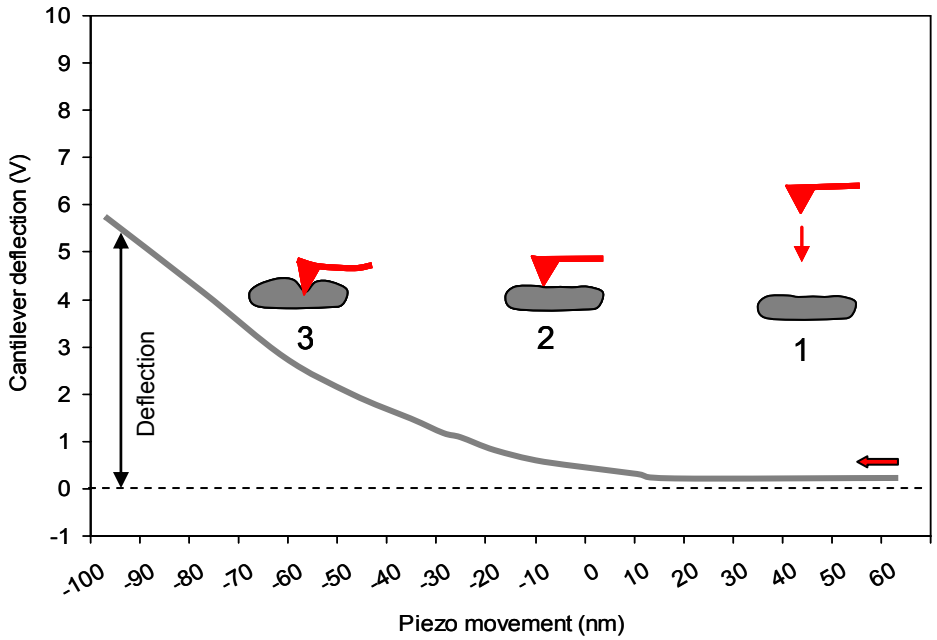


Fig. 9. Schematic of a FD curve on a soft surface.

The cantilever acts as one spring being compressed against another spring, the soft bacterium surface material that is compressed and indented. Thus, the distance of the vertical deflection of the cantilever represents the compression of two springs in a series. To determine the distance of deflection, the Y-axis volts are converted to nanometers using the conversion factor determined in figure 7. In figure 10 the conversion factor has been applied to display the data as nm of cantilever deflection on the Y axis versus piezo distance on the X axis. Each of the voltage points on the Y axis of figure 9 was multiplied by 8, the conversion coefficient.

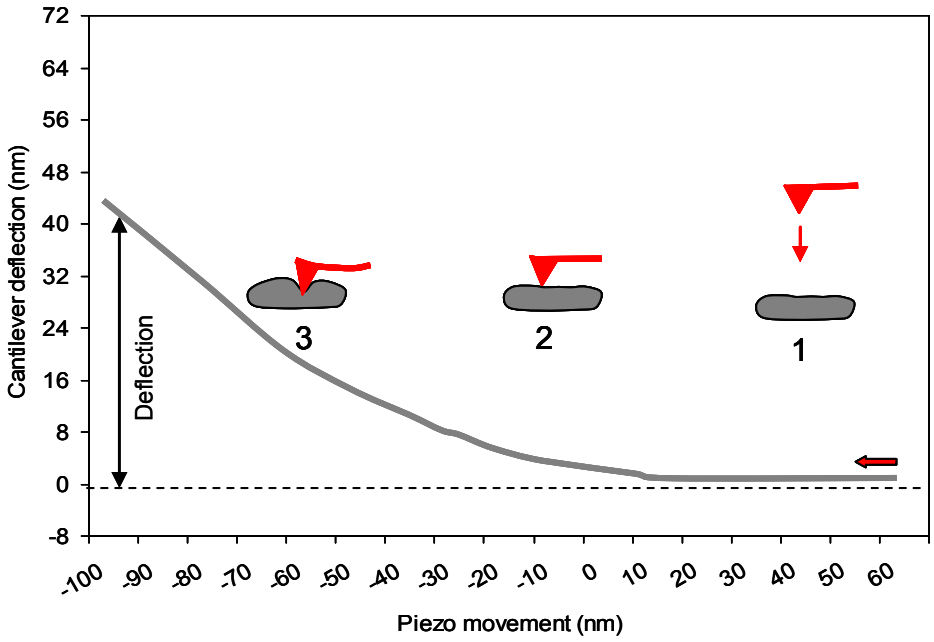


Fig. 10. Cantilever deflection on a soft surface.

Figure 11 shows how the slope of a FD curve taken on a soft surface (gray curve) such as a bacterium is calculated. For FD curves made on bacteria, the overall bacterial spring constant is derived from the region representing indentation of the cell wall. This region can be roughly described as a linear plot, in accordance with Hooke's law and is located at the upper left portion of the curve (Capella et al., 1997; Domke and Radmacher, 1998; Fang et al., 2000; Arnoldi et al., 2000; Almqvist et al., 2001).

The distance that the tip *indents* the bacterium rather than the distance of cantilever deflection must be known to complete the calculation of the bacterial spring constant. The indentation (area indicated by the green arrow) can be

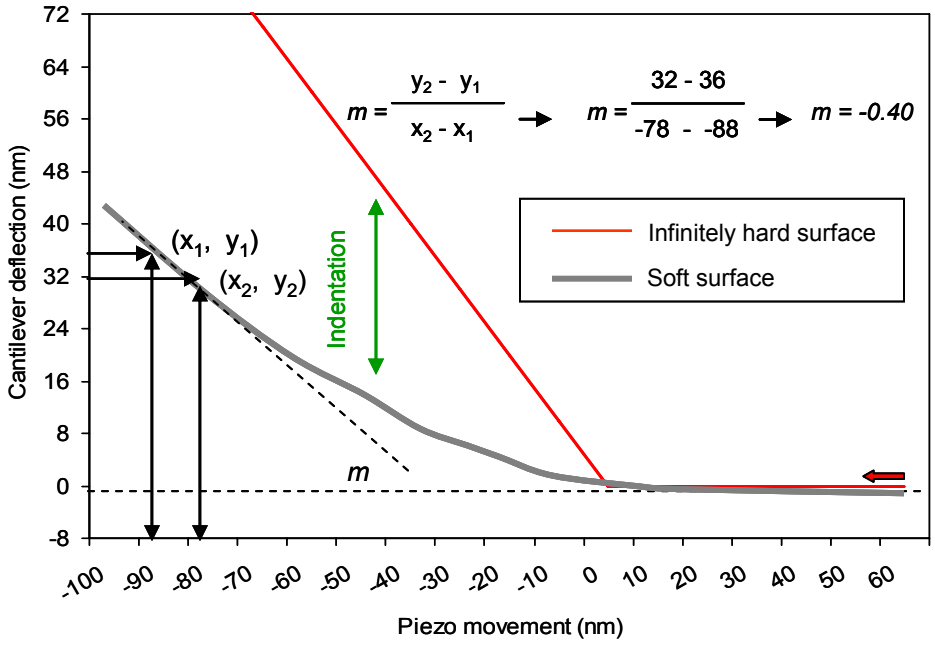


Fig. 11. Tip indentation of a soft surface and calculation of the slope.

calculated by subtracting the distance of cantilever deflection on the bacterium from the total distance of cantilever deflection on an infinitely hard surface (red line) with a theoretical slope of -1 using the equation:

$$k_b = k_c \frac{m}{-1 - m}$$

where (k_b) is the spring constant of the bacterium, k_c is the spring constant of the cantilever, m is the slope of the cantilever deflection versus piezo distance FD curve on the bacterium and -1 represents a cantilever deflection on an infinitely hard surface. By substituting the slope, m = 0.40 and the cantilever spring constant, 0.10 nN/nm in the above formula, the estimated spring constant of the bacterium in these illustrations is 0.07 nN/nm.

3. MATERIALS AND METHODS

3.1 Choice of Mounting Substrate

Muscovite mica was used as the mounting substrate. A hole punch (Ralmikes TOOL-A-RAMA, South Plainfield, NJ) was used to cut ¾ inch diameter mica disks out of flat mica sheets. The disks were cleaved to approximately 0.5 mm thickness using a razor to separate the edges. Clean surfaces of both sides of the disks were exposed by peeling the outer layers off with Scotch tape and clean tweezers were used to manipulate the disks thereafter.

3.2 Preparation of the Mica Disks for Immobilizing EAEC 042

Mica surfaces are negatively charged and hydrophilic. Initial experiments were conducted on EAEC 042 grown in conditions that suppressed expression of the positively charged dispersin coating and AAF, so they too had negatively charged surfaces. The mica disk surfaces were subbed with chrome-gelatin to provide a positively charged surface for bacteria adsorption. A refrigerated stock solution of chrome-gelatin (prepared according to the protocol in the Appendix) was heated to 60° C to reduce the viscosity of the gelatin. Freshly cleaved mica disks were vertically dipped into the warmed chrome-gelatin and supported on edge on a paper towel at a steep angle in a dust free area to air dry overnight.

3.3 Growth of EAEC 042

Bacteria used in this study were the wild type, 042*pet* and the dispersin mutant of the wild type, 042*aap*. The experiments were conducted on four different samples; 042*pet* grown on agar, O42*pet* grown in broth, 042*aap* grown on agar and O42*aap* grown in broth. Bacteria were maintained on Luria-Bertani (LB) broth and these cultures were used to inoculate both LB broth cultures and LB agar plates. Experiments were performed on bacteria recovered at logarithmic phase growth from freshly inoculated broth and solid agar plates that had been incubated at 37° C for 5 hours.

3.4 Preparation of EAEC 042 for AFM

Cells from plate cultures were prepared for imaging by scraping a small quantity of the bacteria off the culture plate with a sterile loop and transferring it into a micro-centrifuge tube containing 0.6 ml of distilled water. The cells were briefly mixed and centrifuged at 10,000 rpm (Eppendorf Centrifuge 5415D, Hamburg, Germany) for 10 min to remove the culture medium before applying them to the gelatin coated mica discs. The wet pellet was suspended in 0.6 ml of fresh distilled water and 100 µl was pipetted onto the center of a gelatin-treated mica disk. The sample droplet was spread to a circular diameter of roughly 5-7 mm then allowed to stand for 10 min for bacterial adhesion. The bacteria mounted disks were then rinsed vigorously in a stream of deionized water to remove non-adherent cells. The disks were then either dried with a focused jet of

nitrogen for imaging in air or covered with distilled water in a liquid cell, as shown in figure 12, for imaging in water.

Cells from broth cultures were prepared similarly starting with 0.6 ml of broth culture and following the procedure described for plated bacteria. Care was taken to insure that once the bacterial samples were removed from their respective growth media, centrifuged to a pellet, and suspended in water, imaging was preformed immediately.

The liquid imaging environment was assembled by placing the bacteria mounted disk in the center of the sample stage (bottom figure) of figure 12 (Molecular Imaging Inc., Tempe, AZ). The liquid cell (top figure) was fitted with an O-ring to protect the stage from leaking water and then clamped over the mica and filled with distilled water. The liquid cell and O-ring were cleaned between samples by sonication (Branson 1510 sonicator, Danbury, CT) for 10 min.

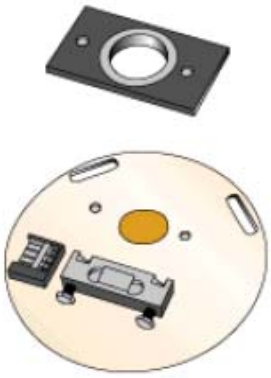


Fig.12. Assembly of liquid cell and sample stage.

3.5 Determination of Cantilever Spring Constant

To verify the manufacturer's quoted cantilever spring constant value for ensuing calculations of bacteria surface elasticity, I used a thermal noise measurement and automatic spring constant calculation software (Thermal K 1.03, Molecular Imaging Inc., Tempe, AZ). A single dedicated cantilever with spring constant of 0.1 N/m was selected for MAC Mode imaging to locate cells and to perform FD curve measurements. Once the cantilever was mounted on the microscope and the laser spot was adjusted on the back of the cantilever for maximum signal onto the position sensitive diode no further adjustments were made for the duration of the experiments.

3.6 Imaging Environments and Modes of AFM Operation

Both air and liquid imaging environments were used; air, to identify unique surface features and liquid, to identify normal appearing bacteria for mechanical measurements. The AFM was operated in the contact mode for imaging in air to investigate surface details and MAC Mode in water to locate cells of normal dimensions for subsequent cell elasticity measurements (Lantz et al., 1994; Han et al., 1996).

3.6.1 Imaging in Air Using Contact mode

Samples of both the wild type (O42*pet*) and the dispersion mutant (O42*aap*) were immobilized on the gelatin-coated mica disks as described in

section 3.5. Nitrogen stream-dried samples were placed in an environmental chamber for imaging where the relative humidity was maintained at 12 % by flooding the chamber with dry nitrogen. Bacteria were imaged using a PicoPlus AFM (Molecular Imaging Inc., Tempe, AZ). Imaging in air was done with the AFM operating contact mode with a scan rate of 1.0 line/second with 512 pixels collected per line. Type II, 225 μm long, bar shaped, MAClever silicon cantilever (Molecular Imaging Inc., Tempe, AZ), with manufacturer's stated nominal spring constants of 2.8 N/m, and pyramid shaped probes 10-15 μm long with tip radii less than 10 nm were used to obtain these images. I began by scanning a large field of bacteria (50 μm x 50 μm) and then I reduced the image size to zoom in on one or two bacteria for higher-resolution imaging. Topographic and deflection images were recorded and the only processing done was first order flattening to remove any vertical offset artifacts between scan lines.

3.6.2 Imaging in Water Using Intermittent Contact Mode

After immobilizatiom on the gelatin-coated mica disks, samples were immediately secured in liquid cells and covered in room temperature, deionized water. Imaging in liquid was done with the AFM operating in MAC Mode with a scan rate of 1.0 line/second with 512 pixels collected per line.

A single, Type IV, 140 μm long, V-shaped, silicon nitride MAClever cantilever (Molecular Imaging Inc., Tempe, AZ) with a pyramid shaped, 3 μm long probe and tip radius of less than 20nm was used to obtain these images and

to conduct FD spectroscopy. The manufacturer's suggested spring constant was 0.1 N/m. Topographic and amplitude images were recorded and the only processing done was first order flattening.

3.6.3 Force Distance Spectroscopy

FD spectroscopy was conducted at the time of imaging in water using MAC Mode. A higher-resolution image containing one or two well isolated, normal appearing bacteria was saved on the computer screen. The topographic image was used to verify that the selected cells exhibited normal heights of at least 600-800 nm for FD spectroscopy. The AFM was then switched from MAC Mode to the contact mode to measure cell elasticity. The X, Y scan size was set to zero and the tip was then centrally positioned over the top of the bacterium. The piezo and cantilever were ramped in the Z direction at sweep duration of 1.0 second and 2000 data points were collected per curve. The amount of force that was applied to the cells did not exceed 10 volts.

Each experiment consisted of collecting two sets of FD curves (25 per set) on two bacteria from each sample. Each experiment was repeated 3 times on separate bacteria cultures.

Topographic imaging was repeated after indentation to make sure that the bacteria did not move while the FD curves were collected. Only indentation data for bacteria with the same height before and after indentation were included in the analysis and both sets of FD curves (25 per set) were conducted on the

same spot. FD curves were also collected on the gelatin-coated mica surfaces next to each bacterium and on bare mica in deionized water, at the beginning, the end and sometimes in the middle of experiments.

3.7 Analysis of FD Curves

Since it is difficult to use the FD curve alone to draw conclusions about the relative softness or stiffness of the various cell layers, we found it helpful to simultaneously analyze the slopes from FD curve raw data files. The raw data that make up the FD curve are provided in a separate spreadsheet file from the FD curve image file. Spreadsheet data are presented in two columns. The first column is a series of piezo movement distances used to plot the X axis. The second column is a series of voltages used to plot the Y axis that represent the tip deflection.

We set the FD curve parameters to collect and plot 2000 X, Y data points from the time the sweep is initiated to the time it is ended. The sweep collected 2000 data points during the approach and indentation of the tip into the bacteria until the cantilever reached the user defined maximum deflection. We used the gradient analysis method described by Li and Logan to analyze the approach region of the FD curves and raw data files (Li and Logan, 2004). A semi-automatic user interface algorithm was developed to analyze FD curves. The algorithm was implemented using MATLAB 7.0.

Using the two sets of FD curves and raw data files that were collected on each sample, an average of the 50 curves was plotted to produce one FD curve that represented each sample. The interface algorithm allowed the user to place the cursor on points of the FD curve in which the slopes appeared to change. Points were selected to divide the curve into 4 different regions (A, B, C, and D). The slopes between consecutive points within each region were instantaneously calculated and plotted on a secondary Y-axis. This allowed us to adjust the 4 different regions according to the calculated slope values and accurately determine where changes in the slopes of the FD curve occurred.

An example of the four separate regions selected is shown in figure 13: (A) a region where the cantilever tip is approaching the sample but has not made contact, (B) a region where there is interaction with the surface without contact, (C) a region where initial contact is made with the surface, (D) a region where hard contact is made with the surface. The raw slope values (un-converted from volts to nm) for the points on the approach curve are plotted on secondary Y axis to the left of the graph. Lines drawn through the upper and lower linear portions of the approach curve are designated *m*1 and *m*2 respectively. The values for the slopes of these lines are indicated by the red arrows located in the centers of regions C and D, -0.1 and -0.2 respectively.

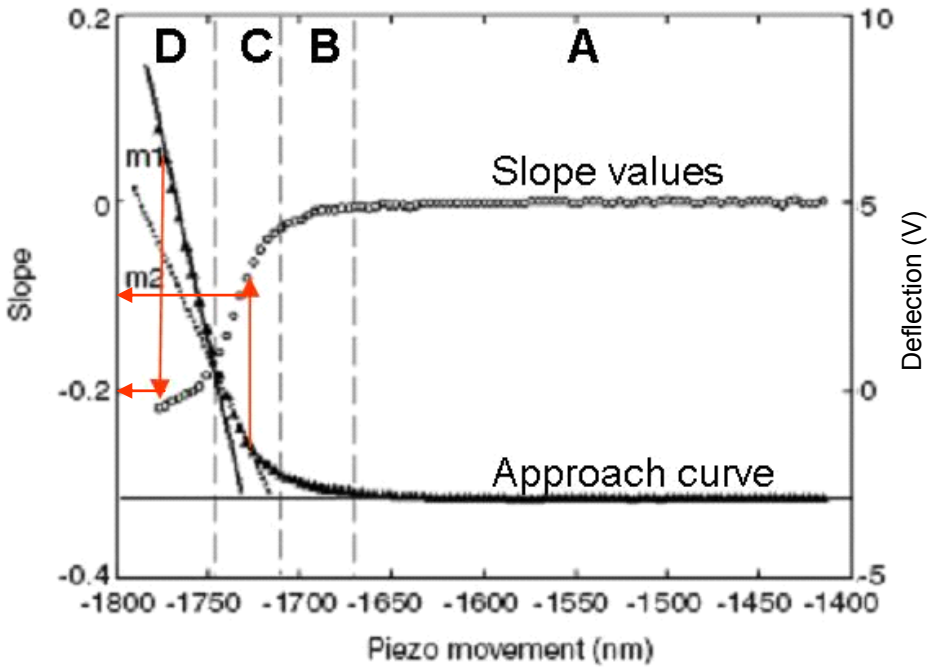


Fig. 13. Example of a FD curve produced by the gradient analysis method.

Once the regions are separated, slopes for each region where linearity is evident can be compared between samples and treatments. The linear region D is thought to be produced when the tip indents the cell wall. The small linear region C might be produced when the tip indents stiff materials of the outer membrane layers described in Chapter 1. Thus, it is possible to compare treatment effects on two different cell envelope structures using one FD curve.

4. RESULTS AND DISCUSSION

4.1 Choice of Mounting Substrate

For AFM, cells must be immobilized on a substrate. The substrate should be flat so that the topography of the cells is easily discriminated from that of the substrate. Mica is the most commonly used sample mounting substrate because it is cheap and has a well ordered crystalline structure and is much flatter than glass. Mica layers can be separated into clean, atomically flat sheets (Zhdan, 1997). The root-mean-square roughness of Muscovite mica, the most common form of mica, is 0.25 Å (Yu and Namba, 1998).

I made ¾ inch diameter disks out of flat mica sheets. Alternatively, squares can be made by cutting the mica with scissors if the sheets are thin enough. I cleaved them no thinner than 0.5 mm in thickness so they would not flex and crack during the bacterial mounting process. If the disks crack the imaging surface will be discontinuous or stepped. By using disks of similar thickness, I was able to limit the tip-sample approach and withdrawal times in between samples. This also prevented cantilever tip damage that can result from switching from a sample mounted on a thin disk to one mounted on a thicker disk.

4.2 Preparation of the Mica Disks for Immobilizing EAEC 042

Most cells are negatively charged and the most common cell mounting surface, glass, is also negatively charged, so mounting cells to a like-charged

substrate is a common dilemma in any type of microscopy work (Vadillo-Rodriguez et al., 2003).To solve this problem, negatively charged substrates are substituted with a positively charged surface (slide subbing) to enhance the adhesion of negatively charged cells.

AFM not only requires that cells be mounted to a solid substrate, they must also be immobilized to guarantee that frictional forces of the scanning tip do not displace them during imaging (Shao et al., 1996). Immobilization should anchor cells without influencing their natural chemistry or morphology. Further, immobilization should be effective in liquid environments that favor viability for imaging and measuring dynamic forces under conditions that are compatible with the natural environment of the cells.

There are a number of immobilization methods for bacteria. Two common methods are mechanical trapping in a filter and physical adsorption (through electrostatic interactions). Mechanical trapping by vacuum filtration is unsuitable for rod-shaped bacteria because they enter the filter holes in such a way that only the ends are accessible to the probe tip. Also, vacuum pressure may deform the cells. For these reasons physical adsorption is preferable because it does not damage the bacteria. A possible disadvantage of this method is it may stimulate the cells to secrete excess extra cellular polymeric substances (EPS) especially if the bacteria are grown on the substrate and form a biofilm (Camesano et al., 2000). EPS is thought to account for higher repulsion forces operating over larger distances upon approach of the AFM tip during force imaging.

I chose the physical adsorption method and used very dilute suspensions of bacteria from broth and agar cultures to limit the possibility of problems associated with EPS secretion.

Of the physical adsorption techniques used in AFM work, the most commonly used is surface subbing with poly–L-lysine. However, I used a chrome-gelatin slide subbing method that was previously developed in this laboratory on the basis of a well established technique for preparing cells for electron and light microscopy (Doktycz et al., 2003). Chrome-gelatin was demonstrated to be superior to poly–L-lysine for immobilizing and imaging both Gram positive and Gram negative bacteria in both air and liquid environments. Another advantage to using chrome-gelatin is that bacteria adsorb to the gelatin within minutes compared to several hours for adsorption to poly–L-lysine (Schaer-Zammaretti and Ubbink, 2003). Also, the collagen protein of gelatin not only modifies the substrate surface charge but is also an adhesive protein for which many pathogenic bacteria, including some *E. coli,* have specific binding sites (Visai et al., 1990). However, it is not known if the EAEC 042 used in this study express these binding sites.

The chromium ions cross-link the large gelatin molecules by coordinate bonds and the adhesive mechanism of the chrome-gelatin is thought to be further enhanced by the formation of coordinate bonds between chromium ions and oxygen atoms on both the mica and bacteria (Kiernan, 1999). It is likely that the

electrostatic interactions and coordinate bonds all contribute to retaining bacteria on gelatin-coated substrates (Sullivan et al., 2005).

We have found that Sigma gelatin (G6144) outperforms other gelatins for the adhesion of bacteria harvested from various growth media preparations (e.g. minimal or supplemented media in solid or broth form) (Doktycz et al., 2003). This was of particular importance in this study since I investigated the effects of two different treatment conditions, broth and agar cultivation.

Both 042*pet* wild type and *042aap* dispersin mutant readily adsorbed to the positively charged gelatin coating of the mica mounting disks. In fact, I occasionally had to repeat the mounting process with more dilute suspensions of bacteria in order to find isolated cells because fewer bacteria than anticipated were washed free during the rinsing step.

In preliminary experiments I cultured 042*pet* in LB broth supplemented with 0.5% glucose to allow the dispersin protein cell coat to be expressed and was not as successful in getting the bacteria to adhere to the gelatin coated mica discs. I attributed this to the positive surface charge that the dispersin protein imparts on the cell's outer surface. Since adhesion was so successful in these baseline experiments in which glucose was not provided to suppress dispersin expression, I am reasonably confident that the FD spectroscopy measurements reflect baseline cell surface characteristics without the influence of dispersin. For future studies when the affects of dispersin protein on the cell surface elasticity are investigated, it might not be necessary to sub the slides.

4.3 Growth and Preparation of EAEC 042 for AFM

Bacteria used in this study were the wild type, 042*pet* and the dispersin mutant of the wild type, 042*aap*. Expression of the dispersin and AAF surface structures is only achieved by growth of 042*pet* in either LB broth with 0.5% glucose, or in minimal essential media (MEM) with high glucose. These structures are not expressed during growth on agar plates. 042*aap* behaves similarly but will express only AAF and the fimbriae will not extend without the dispersin coating (Nishi et al., 2003; Nataro, 2005). I was interested in obtaining baseline cell surface differences between 042*pet* and 042*aap* prior to the expression of dispersin, so I maintained the bacteria on Luria-Bertani (LB) broth and these cultures were used to inoculate both LB broth cultures and LB agar plates. For future studies, when dispersin will be induced to varying degrees by supplementing LB broth with increasing amounts of glucose, we will be aware of inherent differences not attributable solely to dispersin (Nataro, 2005).

Experiments were performed on bacteria recovered at logarithmic phase growth from freshly inoculated broth and solid agar plates that had been incubated at 37° C for 5 hours. This was done to obtain cells that were actively dividing, an indication of viability, so that the images and measurements obtained would be representative of live healthy cells. This also minimized data variability. Stationary phase cultures can be comprised of bacteria at various stages of metabolic activity compared to logarithmic phase cultures with bacteria that are more consistent metabolically.

Cells from cultures were centrifuged and resuspended in water to remove culture medium before attempting to mount them on the gelatin-coated discs. It was previously reported that media contents tend to interfere with bacterial adhesion to surfaces possibly due to competition for surface binding sites (Doktycz et al., 2003).

4.4 Determination of Cantilever Spring Constant

The value of the cantilever spring constant must be known in order to calculate the elasticity (spring constant) of the bacteria cell surface. Manufacturer's quoted spring constant values are useful for initially choosing the type of cantilever for a particular application. However, these values may not be specific enough (range of listed spring constants is too large) for accurate force measurements or they may only be approximate values. A comparison of calibration methods for various types of AFM cantilevers from different batches indicated that spring constant values could vary by as much as 20% from manufacturer's suggested values (Burnham et al., 2003).

It is difficult to complete an experiment involving multiple samples and replicate measurements using a single cantilever due to the delicacy of the tip. Ideally, replacement cantilevers will have the same spring constants as the original cantilever. If not, then spring constant differences of each cantilever used must be known. There are a number of calibration methods for verifying cantilever spring constants. These methods are either based on cantilever

geometry, thermal properties or comparisons between the cantilever stiffness and reference materials of known stiffness (Cleveland et al., 1993; Hutter and Bechhoefer, 1993; Burnham et al., 2003).

Thermal property analysis is the simplest and least tip-destructive of these methods. This method takes advantage of the fact that thermal fluctuations in the environment (air or water) provide small force impulses that can diffuse small particles (Brownian motion). Soft cantilevers are also susceptible to these thermal fluctuations which can be measured by the AFM using the same set-up as for imaging. A thermal noise spectrum plots the oscillations of a cantilever as a function of frequency. The greatest amplitude of these oscillations will be at the cantilever's resonant frequency. The amplitude of the oscillations for a given temperature depends only on the spring constant of the cantilever (Hutter and Bechhoefer, 1993; JPK Instruments, 2006).

I used a thermal noise measurement and automatic spring constant calculation software (Thermal K 1.03, Molecular Imaging Inc., Tempe, AZ) to compare spring constants of cantilevers from the same batch and found that the spring constants varied about 20% on average from the value reported by the manufacturer (data not shown). When the same cantilever was calibrated repeatedly, individual spring constant values were all within 5% of the average value.

The measured deflection distance of the cantilever not only depends upon the cantilever spring constant, but also on the optical path of the AFM detection

laser. A drawback to replacing cantilevers in the middle of an experiment is that the optical path will be slightly different with each cantilever placement because it is difficult to replace one cantilever in the exact position as the last one (JPK Instruments, 2006). Therefore, to optimize the signal between cantilevers the laser must be repositioned on the back of each successive cantilever. Differences in cantilever position not only impact the location of the laser spot on the photodiode but also the quality of the laser spot and ultimately the measurements (Dcosta and Hoh, 1995).

I anticipated that the differences in elasticity would be small for our initial baseline measurements between the wild type 042*pet* grown in dispersin suppressive conditions and the dispersin mutant, 042*aap*. Therefore I did not think that the 20% spring constant variability between cantilevers was acceptable because small elasticity differences could be masked by cantilever and optical pathway differences.

In considering the amount of error that could be introduced by replacing cantilevers, I reasoned that the best approach would be to set up the experiments in a way that would conserve the use of a single cantilever. By using a dedicated cantilever for FD curve measurements, experimentally measured values of slopes could then be attributed to differences in bacteria alone rather than differences in cantilever spring constants or laser positions. Once the cantilever was mounted on the microscope and the laser spot was adjusted on the back of the cantilever for maximum signal on the position sensitive diode, no

further adjustments were made for the duration of the experiments.

Based on my review of literature, typical spring constant values of Gram negative cell walls range from .03 to .07 N/m, so I selected a cantilever with a spring constant of 0.1N/m that would be sensitive enough to deflect in response to the soft bacteria surface and yet stiff enough to indent the cell wall (Arnoldi et al., 2000; Yao et al., 2002; Velegol and Logan, 2002).

4.5 Imaging Environments and Modes of AFM Operation

I used both air and liquid imaging environments; air, to identify unique surface features and liquid, to identify normal appearing bacteria for mechanical measurements.

The contact mode was used for imaging in air because even dry surfaces are coated with a layer of water. In the MAC Mode this can be problematic because capillary action between the tip and sample water layers continually brings the tip and sample into contact even when the chamber is flooded with dry nitrogen to reduce the amount of water that condenses between the tip and sample. Prolonged tip-sample interactions interfere with the amplitude of the oscillating tip over the surface and interrupt image acquisition.

A drawback in using the contact mode is the tip is subject to permanent damage or accumulation of debris from its contact with surfaces. Tip damage or tip fouling changes the conformation and performance of the tip. Images artifacts can result from tip changes, but these are usually apparent when viewing the

image. More important is the influence that a change in tip conformation may have on FD curves. In this case, the impact on the shape and slope of the FD curve may not be obvious and could lead to erroneous conclusions regarding cell elasticity. Additionally, the contact force can also damage or change the natural conformation of the cell surfaces or dislodge the sample from the surface.

Therefore, I also used the MAC Mode for imaging in water to get the topographic images and complement the data obtained by contact mode imaging in air and to preserve the tip dedicated for force imaging. This mode of operation uses the least amount of tip force on the sample. For ensuing elasticity measurements with FD spectroscopy it was important to be able to use the same tip for comparative analysis.

In summary, I used the contact mode for imaging in air to investigate surface details and MAC Mode in water to locate cells of normal dimensions for subsequent cell elasticity measurements (Lantz et al., 1994; Han et al., 1996).

4.5.1 Imaging in Air Using Contact Mode

The samples were dried and images were taken in contact mode in a humidity controlled environment. These AFM images of both the 042*pet* wild type and *042aap* dispersing mutant are presented in figure 14.

One of the effects of drying can be clearly seen in the topographic image (a) of 042*pet* grown on agar. In this image the cross section height of the bacteria shown in both the line scans (f, g) is roughly 200-300 nm as opposed to the

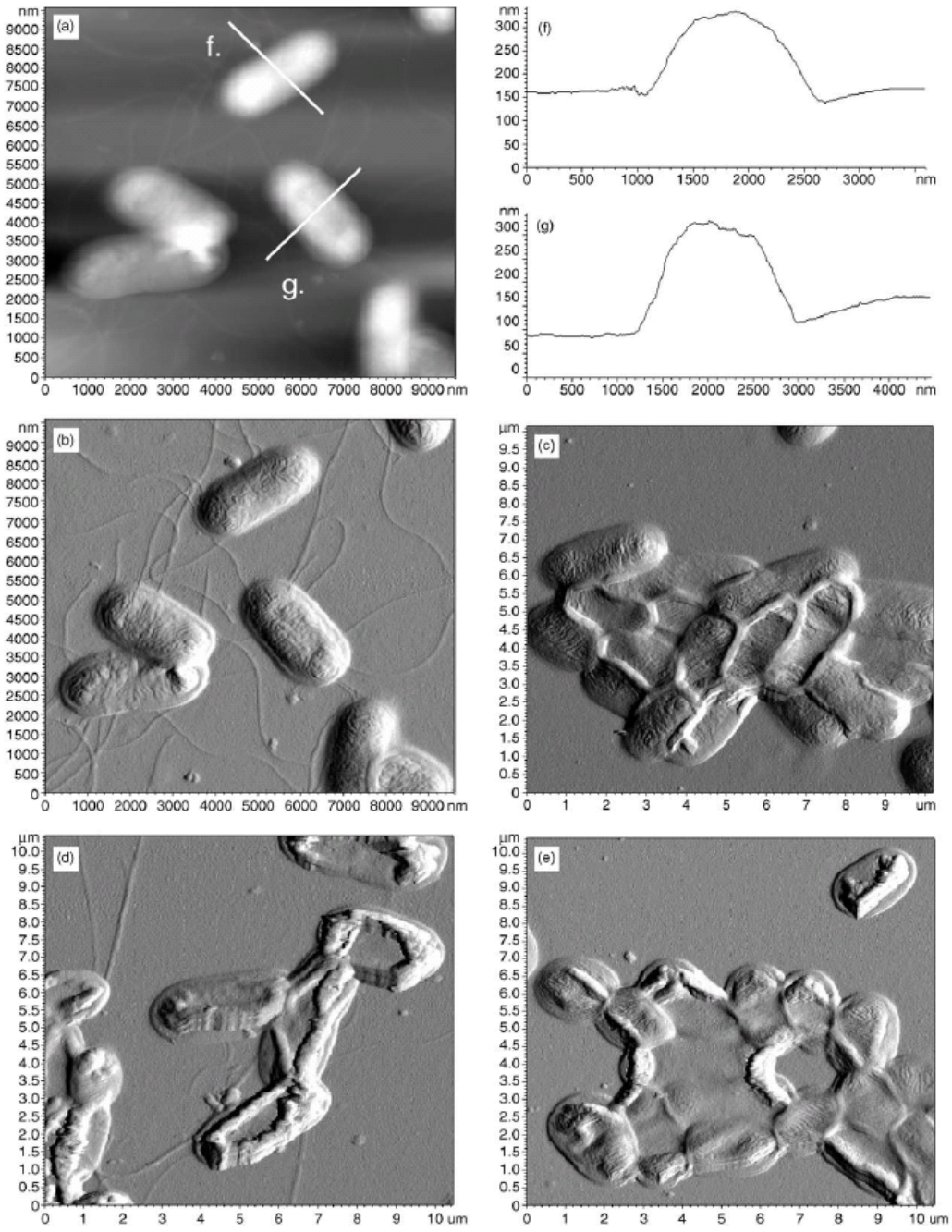


Fig. 14. Contact mode images in air. Scale bars are shown on the X and Y axes.

height measured in liquid of 600-800 nm. Similar effects of drying were seen for the other dried preparations. This apparent difference is due to dehydration and indicates that the bacterial cell wall lacks the rigidity to maintain its form when water is removed. Deflection mode images of 042pet grown on LB agar (b) and in LB broth (d) and 042aap grown on LB agar (c) and in LB broth (e) show a marked dehydration of the bacteria without lysis.

In deflection images (b-e), true height values that are discernable in topographic images are sacrificed to allow for a more comprehensive view of the entire cell structure from the gelatin substrate to the top of the bacteria. For example, structures that appear to be flagella can be seen lying on the substrate surface near the bacteria. 042*pet* have flagella when grown both on agar (b) and in broth (d), although more evidence of flagella when grown on agar, while *042aap* do not exhibit any flagella when grown either on agar (c) or in broth (e). We found that when cells are isolated they tend to maintain their rod-like shape while cells in close contact show a more pronounced collapse of the cell wall. This is clearly seen in (b) where the isolated cells of 042*pet* grown in agar are more normal looking as opposed to (c) where *042aap* grown in agar shows a normal looking cell on the periphery but the closely packed cells definitely show evidence of severe dehydration. One observation that we have made in comparing images of all different preparations is that cells grown on agar appear to maintain their characteristic rod shaped appearance better than cells grown in broth. This can also be seen in the images where 042pet (b) and 042aap (c) on

agar appear to be less dehydrated than (d) 042pet and (e) 042aap grown in broth.

4.5.2 Imaging in Water Using MAC Mode

AFM imaging of cells in liquid was accomplished using MAC Mode. In figure 15, topographic images of all four of the bacterial sample preparations are shown imaged in water. The EAEC 042*pet* wild type is shown grown on agar (a) and in broth (c) while the dispersin mutant 042*aap* is shown grown on agar (b) and in broth (d) respectively. Logarithmic cultures were used as evidenced by the presence of dividing cells (red arrows) in all the images. There appears to be very little morphological differences in these images. This is expected because the depth of field of the topographic image does not allow the entire height of the bacteria to be imaged while also including structures that might exist on the lowest part of the image. For example, pili, or flagella that might be present on the gelatin substrate surface would not be seen in the topographic image. A line was arbitrarily drawn across the image to show the topography of the sample as a function of distance. Line scans (e–h) taken through their corresponding images (a–d) show an average height of 600–800 nm. A line scan that passes perpendicularly across bacteria shows an exaggerated width of roughly 2 microns. This is due primarily to the tip being shaped as a pyramid such that a convolution of the image results (Radmacher, 1997).

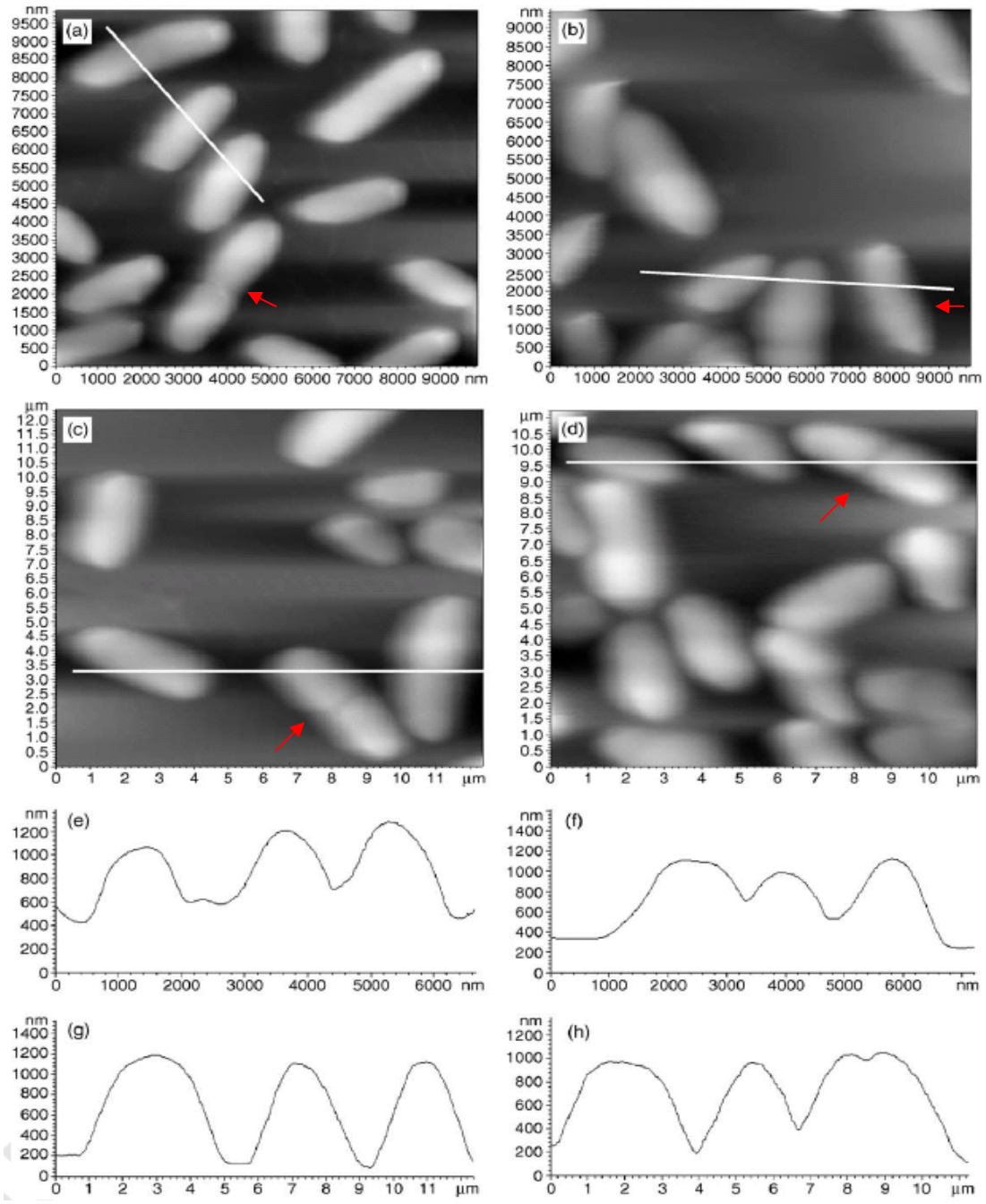


Fig. 15. Topographic Mac Mode images in water. Scale bars are shown on the X and Y axes.

4.6 Force Distance Spectroscopy

Figure 16 shows bacteria images before (left) and after (right) FD spectroscopy to demonstrate that the bacteria did not move while FD spectroscopy was performed. This is evidenced by the unchanged proximity and orientation of the cells to one another. The cross section line (green) shows that the height of the bacteria did not change after FD spectroscopy, indicating that the bacteria were not damaged. There is, however, some piezo drift (about 3 µm in the Y direction and about 1 µm in the X direction) during the 24 min time lapse between the before and after scans. This emphasizes the importance of rescanning between FD spectroscopy on the same bacteria over an extended duration to make sure that the cursor can be placed in the exact desired location

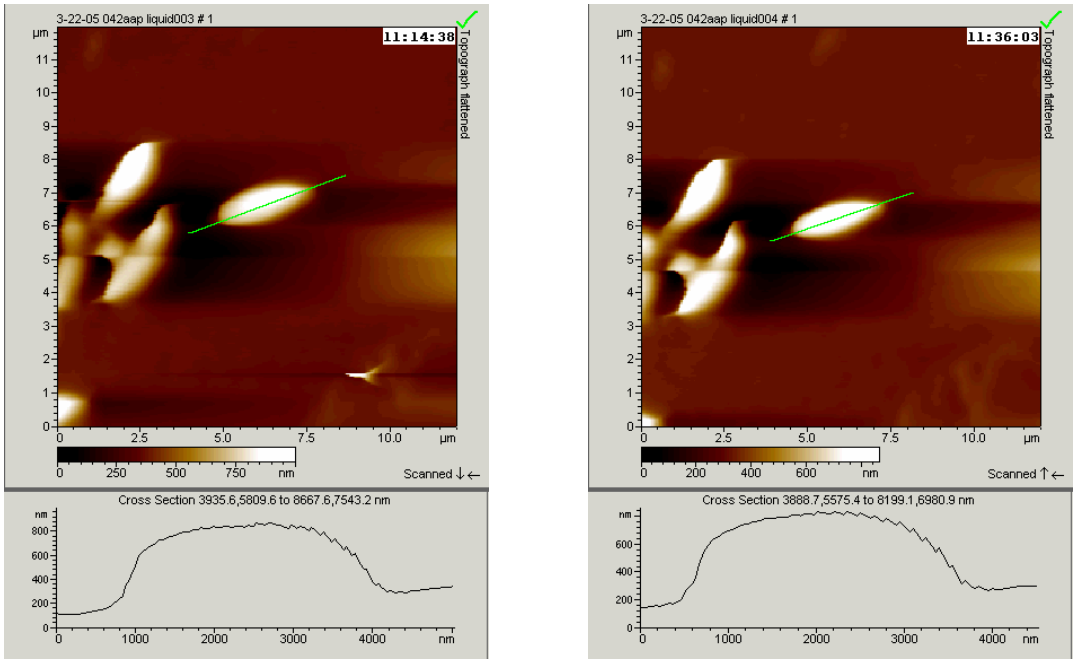


Fig. 16 Images before and after FD spectroscopy.

each time. As testimony to the gelatin immobilization technique, this particular image was produced in water using the contact mode, not the intermittent contact mode.

The purpose of a FD curve is to reveal regions of linearity and non-linearity. Linearity occurs where there is a predictable increase in cantilever deflection per increase in piezo distance indicating resistance or stiffness. Non-linearity occurs where there is an unpredictable increase in cantilever deflection per increase in piezo distance indicating compliance or softness. The greater the slope value, the harder the surface. The slopes of the linear regions on the FD curve are used to derive spring constants of the materials encountered by the tip. For instance, raw FD curves made in water on bare mica, bare gelatin and a bacterium are shown in figures 17, 18, and 19, respectively. The slopes are indicated on the lower right with a purple circle. The slopes on mica and gelatin are the same, 0.208, while the slope on the bacterium is 0.097 indicating that the mica and gelatin substrates are harder than bacteria.

The bacterium's effective spring constant, the integral characteristic of the cell as a whole, is typically derived from the value of the slope of uppermost linear region of the FD curve. This region of the FD curve is created when the tip finally reaches and presses on the peptidoglycan layers of the cell wall.

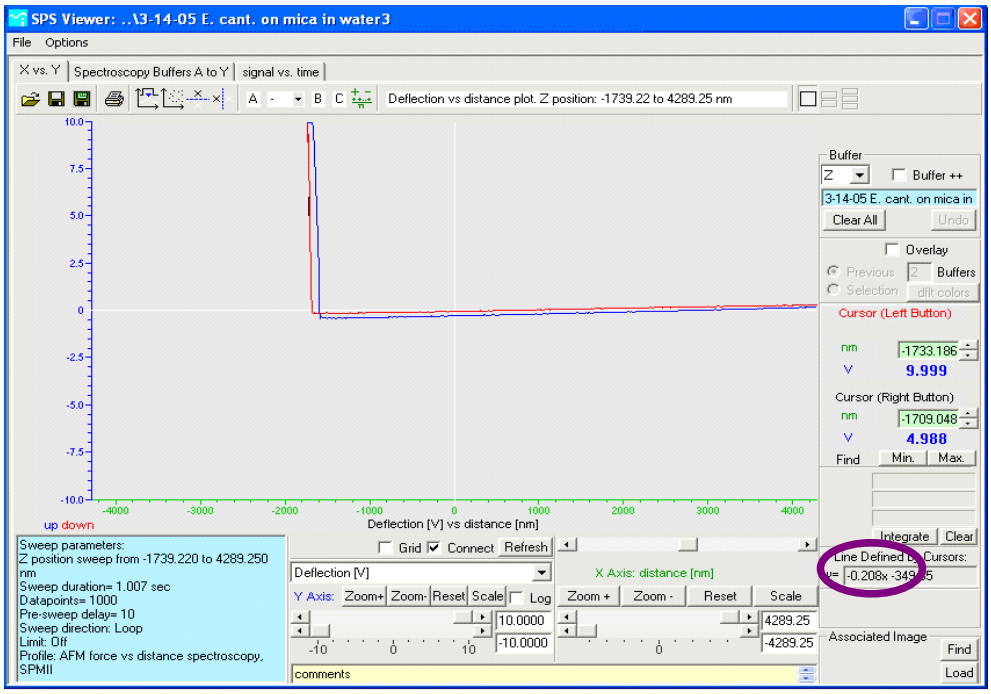


Fig. 17. Raw FD curve made in water on bare mica.

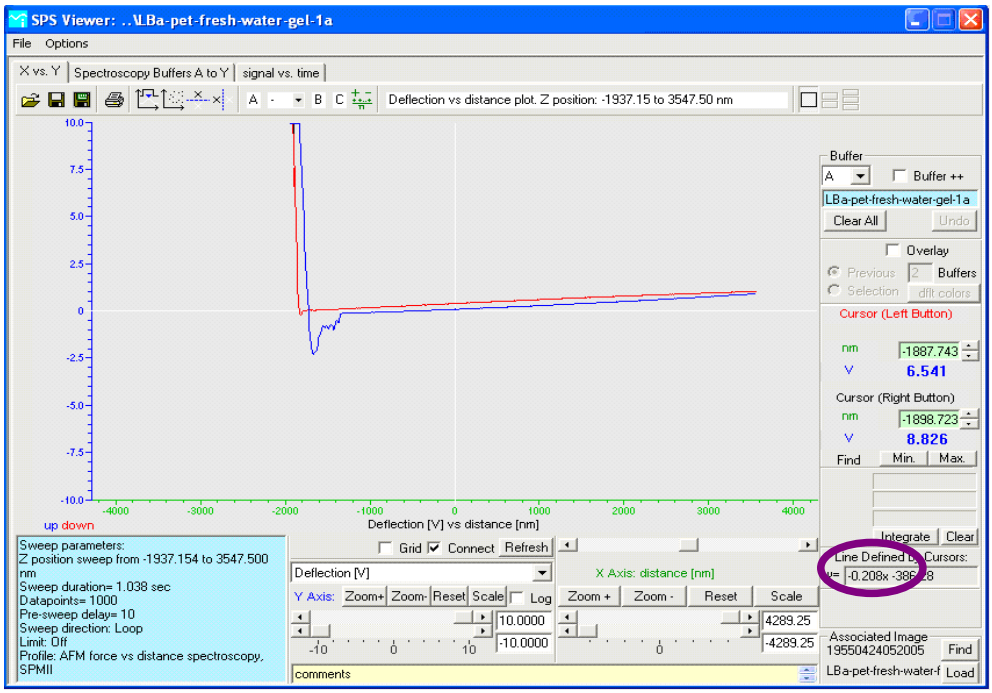


Fig. 18. Raw FD curve made in water on bare gelatin coated mica.

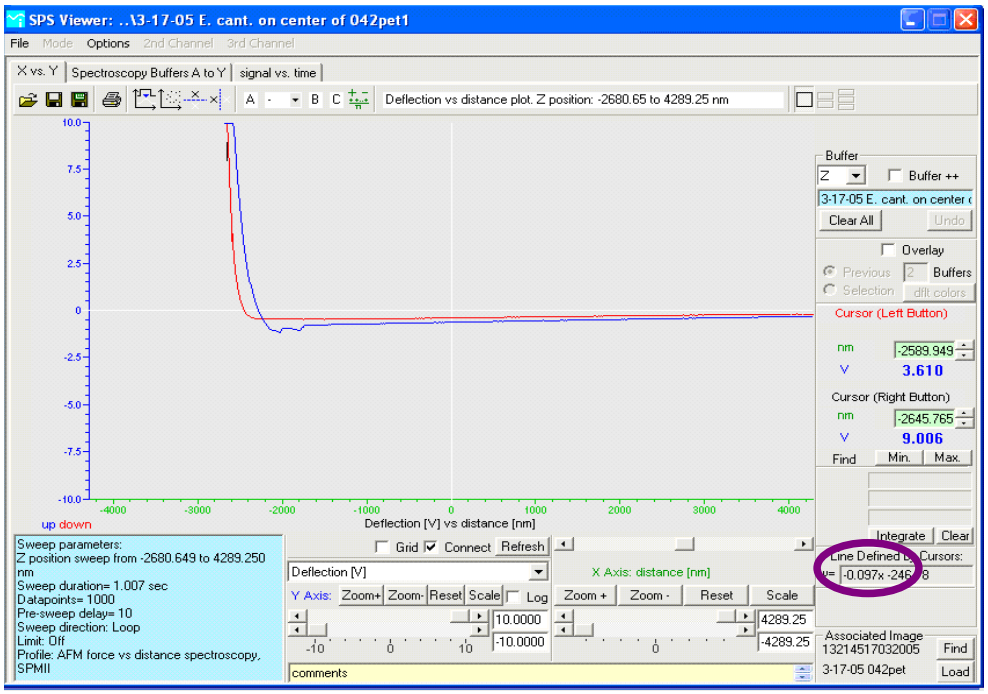


Fig. 19. Raw FD curve made in water on a bacterium.

However, by using the gradient analysis technique, we have also noticed that a linear region is also apparent at the point of contact between the tip and the outer cell envelope surface layers. We believe that this first linear region may provide additional information about other components of bacteria cell envelope composition.

This first linear region is not usually discernable by visual analysis of the FD curves alone. The problem is that the AFM does not provide direct measurement of the distance between the sample and the tip, so the determination of “zero” axes is a very complicated problem. The exact distance is difficult to determine for two reasons. The first reason is that just before physical

contact electrostatic repulsion causes the cantilever to begin deflecting away from the sample. The second reason is that Gram-negative bacteria are covered with multiple layers of material with varying degrees of softness.

These initial surface interactions make it difficult to separate the areas of the FD curve that represent the cantilever's response to each different cell layer from the area that represents the actual indentation of the bacterium. To illustrate, the bracketed area of figure 20 shows the approach portion of a FD curve made on a *042pet* bacterium from an LB broth culture. Without the benefit of the cantilever diagrams over the curve, such as those shown in figure 7, it is difficult to define the exact zero axis –where the cantilever indents the bacterium. In the bracketed area the cantilever may be experiencing electrostatic repulsion (non-linear), or it may be pressing into the softer outer envelope layer (linear or non-linear depending on the material) or actually beginning to indent the cell wall (linear). Large uncertainty in the exact location of linear regions leads to significant variation in the estimation of the elasticities of a cell envelope's layers.

Since it is difficult to use the FD curve alone to draw conclusions about the relative softness or stiffness of the various cell layers, we simultaneously analyzed the slopes from FD curve raw data files. We used the gradient analysis method described by Li and Logan to analyze the approach region of the FD curves and raw data files (Li and Logan, 2004).

Using the 2 sets of FD curve image and raw data files that were collected on each sample, an average of the 50 curves was plotted to produce one FD

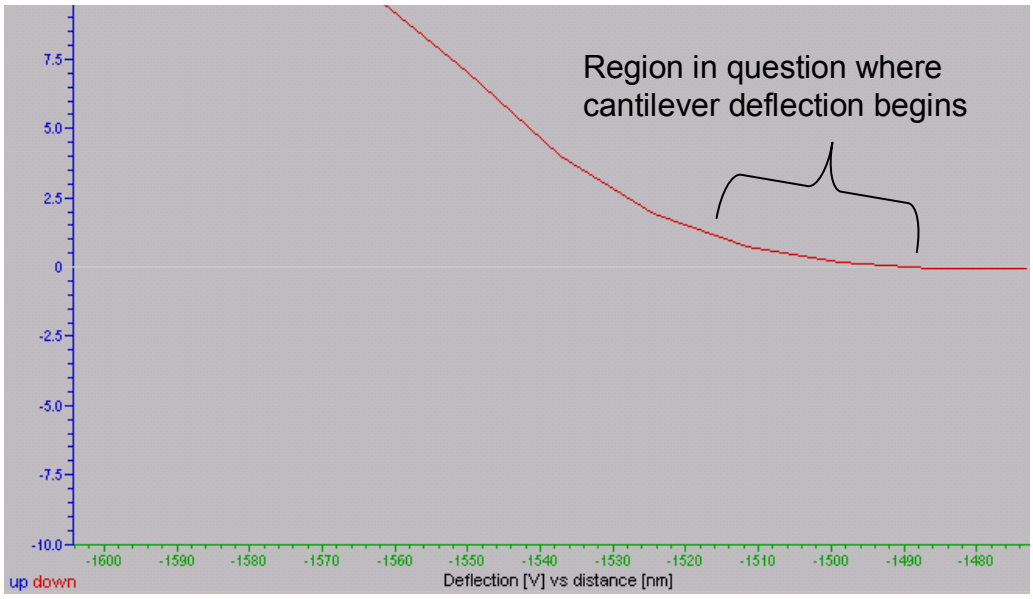


Fig.20. An approach portion of a raw data FD curve on a bacterium.

curve that represented each sample. These experiments were repeated three times and the results for each sample were in agreement. The results of one of the experiments are presented in figure 21. These are raw FD curves of volts versus piezo distance, but the slopes can still be compared to one another since the same cantilever was used.

In all of our experiments force measurements were made with the sample in water and a bare mica surface in water was used as a control. Force measurements were made on mica before, midway and at the end of the experiment to determine if there was any change in the spring constant as evidenced by a change in slope. For example, in the data presented in figure 21 (a), the slope (*m*1) for mica was 0.223, 0.235, and 0.217 respectively for the

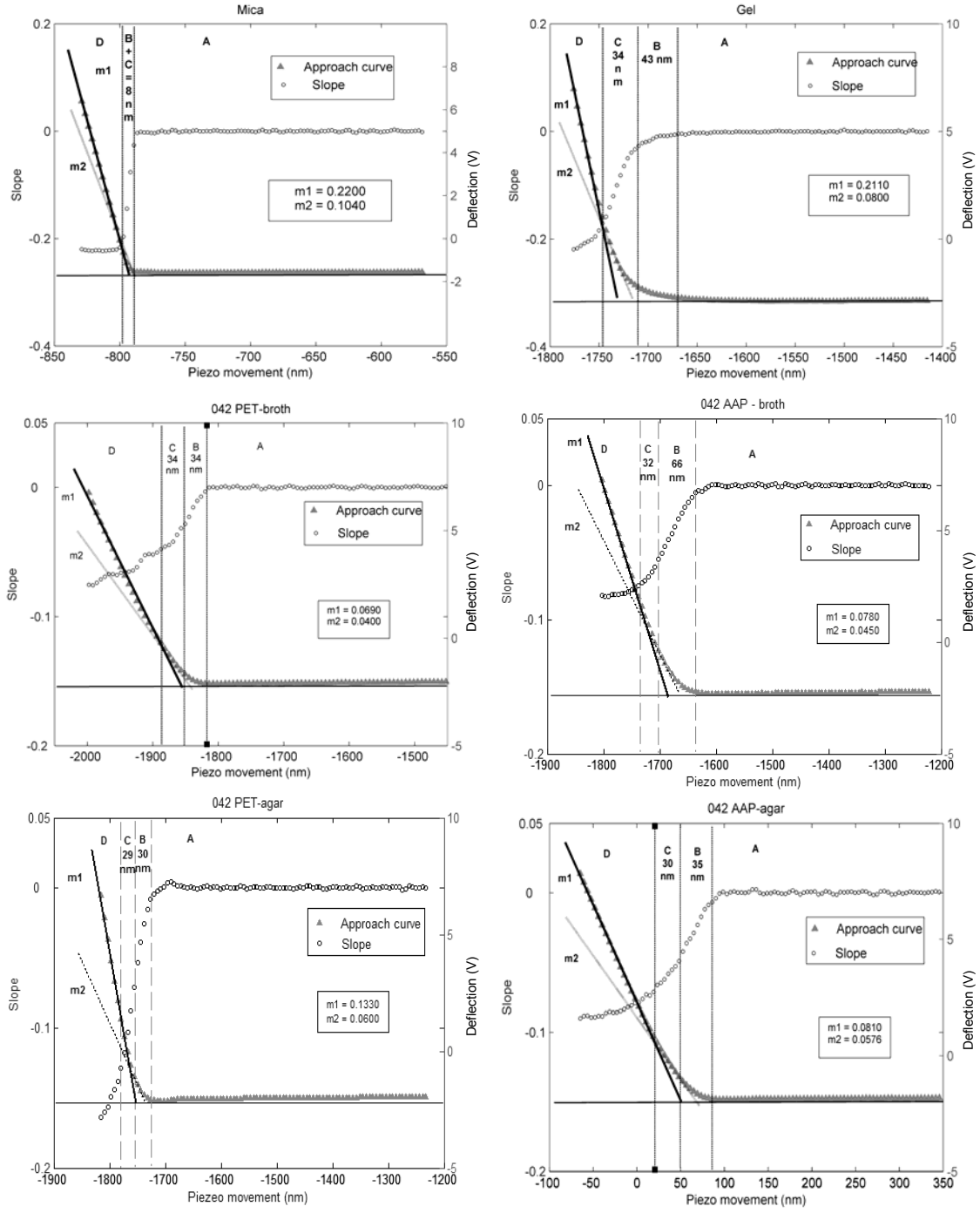


Fig. 21. The approach portions of experimental FD curves.

beginning, midpoint, and end of the experiment. Therefore, the AFM consistently measured the cantilever and bacterial spring constants within an acceptable degree of error (0.009).

In each FD curve of figure 21, regions A all show the approach of the cantilever tip to surface. The approach curves in these regions are all flat and the corresponding calculated gradient slopes are zero. On the FD curve of bare mica (a), region B is difficult to differentiate from region C where initial contact with the surface is made. By visual inspection alone it appears that the tip is sharply deflecting at contact with the surface. This is a good indication that sweep parameters chosen to minimize hydrodynamic drag were appropriate otherwise there would be a longer distance of piezo movement per increase in deflection. However, the gradient analysis detected the difference in slope in this region and indicated that there is a cantilever deflection of 8 V that before the tip makes hard contact with the surface. This demonstrates that our gradient analysis technique is extremely sensitive and improved our ability to identify changes in slopes in this difficult region. The FD curve on bare mica is a good control and serves as a reference curve for determining the conversion factor (discussed in Chapter 2) which was 3.3 nm per V.

Regions B on the gelatin in figure 21 (b) and bacteria FD curves (c-f) are well differentiated. This is because the tip underwent electrostatic repulsive interactions with the gelatin/bacteria surfaces just before contact. The tip might also be being deflected by soft, flexible structures external to the cell walls such

as fimbriae, pilli, and flagella (Dufrene et al., 2001; Vadillo-Rodriguez et al., 2003).The approach curves and slopes in these regions are all non-linear. It is not clear what caused the cantilever to deflect more in region B (66 V) of the *0*42*aap* dispersin mutant grown in broth (d) than the other bacteria (30-35 V). *0*42*aap* does not express the dispersin surface protein and all bacteria were grown in conditions known to suppress dispersin and AAF expression. Only the 042*pet* displayed flagella. Another known cause for increased cantilever deflection at this region is EPS secretion. However, I have no reason for thinking EPS was the cause since all of the samples were treated similarly. Future research may reveal interactions other than those known to cause tip deflection at this point in the FD curves of 042*aap*.

Of primary interest are regions C, where the tip indents the bacteria's outer surface, and regions D where the tip presses into the cell wall. These regions contain areas of linearity where the distance traveled by the sample toward the tip is proportional to the tip deflection. The *m*1 slope has traditionally been used to determine relative stiffness or elasticity of the bacterial cell wall (Radmacher, 1997; Arnoldi et al., 1998; Dufrene et al., 2001; Velegol and Logan, 2002; Bukharaev et al., 2003; Bolshakova et al., 2004). The *m*2 slopes could represent the indentation of the outer cell surface layers.

In regions C, the slopes (*m*2) are calculated over similar distances of cantilever deflection for all four bacteria samples. Given the amount of standard deviation in spring constant measurements (0.009) determined on the bare mica

control, the values for *m*2 are equal for 042*pet* (*m*2 = 0.040) and *0*42*aap* (*m*2 = 0.045) grown in broth. These values are also equal for 042*pet* (*m*2 = 0.060) and *0*42*aap* (*m*2 = 0.057) grown on agar. This indicates that dispersin expression which is anticipated to affect the outer cell wall elasticity was successfully suppressed for these baseline measurements. The *m*2 values do show that surfaces of bacteria grown on agar have greater rigidity compared to surfaces of bacteria grown in broth. These differences in slope values between agar and broth-grown bacteria surfaces support our observation that agar-grown cells appear less dehydrated than do the broth-grown cells imaged in air shown in figure 14.

The upper-most portion of the FD approach curve, region D, is most often used to calculate the whole bacteria spring constants. Looking at the slopes of *m*1 for all the surfaces we conclude that mica is definitely the most rigid surface followed by gelatin-coated mica that serves as a substrate for mounting the bacterial samples. The values for *m*1 are slightly different between 042*pet* (*m*1 = 0.069) and *0*42*aap* (*m*1 = 0.078) grown in broth. These values are also different between 042*pet* (*m*1 = 0.133) and *0*42*aap* (*m*1 = 0.081) grown on agar. By comparing *m*1 values, we found that the different growth conditions, on agar or in broth, only affected the cell wall rigidity of the wild type, 042*pet*. There is no difference in the slopes of *0*42*aap* grown on agar and in broth. Therefore, the cell walls as well as the outer cell layers of 042*pet* are sensitive to the two different

growth conditions, while only the outer cell layers of *0*42*aap* were affected by the growth conditions.

Experimental spring constant values are useful in that they allow universal comparisons to be made across studies. For instance, the bacteria cell wall spring constants from this study are presented in table 1 and all are within range of spring constants reported by others for Gram negative bacteria and. For instance, *E. coli* K12 strains were found to have cell wall spring constants of 0.037 N/m when mounted on Poly(ethyleneimide) (PEI) coated glass slides (Velegol and Logan, 2002). *Pseudomonas aeruginosa*, mounted by vacuum through a filter followed by drying and then rehydration, had cell wall spring constants ranging between 0.02 and 0.03 N/m (Yao et al., 2002). *Magnetospirillum gryphiswaldense* mounted on silane trimethoxysilyl-propyl-diethylenetriamine (DETA) coated glass slides had cell wall spring constants ranging between 0.04 and 0.07 N/m (Arnoldi et al., 2000).

Table 1. Spring constants were derived for cell wall and outer cell envelope using the slopes *m*1 and *m*2, respectively.

Bacteria/growth condition	Spring constant (nN/nm) of cell wall (from *m*1 slope)	Spring constant (nN/nm) of outer cell envelope (from *m2* slope)
042*pet* (broth-grown)	0.04	0.02
042*pet* (agar-grown)	0.07	0.03
042*aap* (broth-grown)	0.03	0.02
042*aap* (agar-grown)	0.04	0.02

The slopes from which these spring constants were derived were calculated from the X, Y coordinates of the FD curves in figure 21. The Y axis values were converted from volts to nanometers using the conversion factor 3.3 nm/V as described in Chapter 2. The conversion factor was determined from the FD curve on bare mica in figure 21.

5. CONCLUSIONS AND FUTURE EXPERIMENTS

The bulk of this research was directed at further establishing a mounting technique for effectively immobilizing bacterial cells for extensive physical AFM experiments, and developing a fast and highly informative means of analyzing the FD curves. The gelatin mounting technique was previously demonstrated in this laboratory to be a superior immobilization strategy and this research demonstrated that it is also effective during force spectroscopy. Prior to the use of the gradient analysis algorithm, we were unable to identify the second region of linearity that may represent the outer membrane elasticity because the FD curves are difficult to analyze visually.

We have used these immobilization and gradient analysis techniques to record AFM images and report force measurements on a pathogenic strain of enteroaggregative *Escherichi coli* (EAEC) that produces a severe diarrhea in humans. The wild type strain 042*pet* produces a protein, dispersin, that is implicated in pathogenesis. In this thesis a mutant of 042*pet* that does not produce dispersin, 042*aap,* is compared to the wild type grown in dispersin suppressive conditions to determine if any baseline physical differences exist before investigating differences caused by dispersin expression. We have found some differences in morphology and cell rigidity between the two strains and will investigate in future research the added impact of dispersin expression to these differences that could implicate this protein in the pathology of this bacterial strain.

The full expression of dispersin *in vitro* is dependent on two environmental factors. EAEC 042 must be grown in broth culture and the culture must contain at least 0.5% glucose. It is possible that dispersin may be expressed to a limited degree in lower concentrations of glucose. To investigate the influence of the dispersin protein more thoroughly, future research with EAEC 042 should include growth in minimum essential media (MEM) with gradually increasing concentrations of glucose (e.g. a glucose gradient from 0-0.05%).

LB media used in these experiments may contain a slight amount of glucose from the ingredient yeast extract. Glucose is primarily a component of the yeast cell wall. The cell wall is excluded in most yeast extract processing but preparations vary from batch to batch and the absolute ingredient concentrations are not guaranteed. To be absolutely sure that the differences found in this research between the cell wall elasticities of broth grown cultures of 042*pet* (0.0074 N/m) and 042*aap* (0.0084 N/m) were not due to dispersin, these experiments should be repeated on these bacteria from MEM cultures with no glucose supplementation should be investigated. FD spectroscopy performed on EAEC 042 in which dispersin is expressed will reveal whether or not this protein is soft or hard and what the effects of secretion of dispersin have on the constitution of the cell wall.

It would also be interesting for future experiments to address the extent of coverage of fully expressed dispersin. Figure 22 shows a scanning electron micrograph of 042 *pet* in which the AAF unique to EAEC is indicated with a black

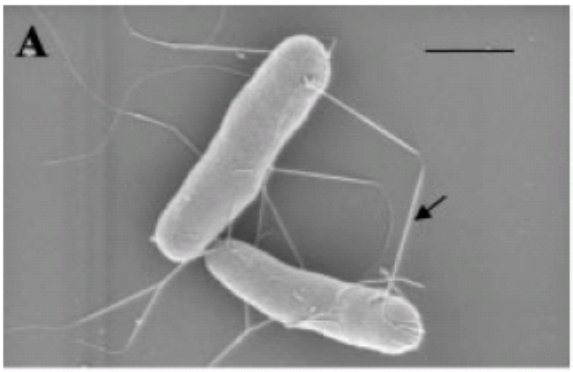


Fig. 22. A scanning electron micrograph of 042*pet*.

arrow. What distinguishes the AAF from the flagella is its straight rather than curved configuration. The straight appearance is thought to be caused by tension in the fimbriae which functions as an anchoring appendage. In some locations the AAF appear to be lying across the cell surfaces. This is cause to question the continuity of the dispersin coating across the cell surface. The positively charged dispersin protein must be expressed to allow the positively charged AAF to extend from the bacterial surface. Therefore, it seems unlikely that we would see the AAF tethered over the top of neighboring cells unless there are patches of negatively charged LPS exposed to allow this to happen.

The elastic property and extent of surface coverage of dispersin could be investigated by two methods, microelastic mapping and molecular recognition force microscopy (MRFM). A microelastic mapping is a mode of high-resolution visualization in which the image contrast is based on the mechanical properties of the sample rather than the topography (A-Hassan et al., 1998). By collecting

arrays of FD curves over the entire cell surface instead of single measurements at select locations, two dimensional maps of whole cell mechanical properties can be produced. Images produced are similar to topographic images where gray scales indicate low areas with dark gray and high areas with light gray. Microelastic maps reveal stiff areas as dark and soft areas in light gray.

The stiff or soft areas can be correlated with areas of dispersin location through MRFM. In MRFM an antibody is attached to the tip of the cantilever that is specific for the surface antigen and images are simultaneously collected with force recognition images (Allison et al., 2002). In this case an antibody for dispersin is available for the dispersin antigen. As the tip is scanning the surface it is magnetically oscillated to and from the surface in the Z direction. When the tip reaches the surface, binding events occur between the antibody and antigen; then as the tip moves away from the surface unbinding occurs. The force recognition images are produced by unbinding events when the tip retracts from the surface.

LITERATURE CITED

1. Yao X, Jericho M, Pink D, Beveridge T, 1999. Thickness and elasticity of gram-negative murein sacculi measured by atomic force microscopy. Journal of Bacteriology 181: 6865-6875.

2. Yao X, Walter J, Burke S, Stewart S, Jericho MH, Pink D, Hunter R, Beveridge TJ, 2002. Atomic force microscopy and theoretical considerations of surface properties and turgor pressures of bacteria. Colloids and Surfaces B-Biointerfaces 23: 213-230.

3. Vadillo-Rodriguez V, Busscher HJ, Norde W, de Vries J, van der Mei HC, 2003. On relations between microscopic and macroscopic physicochemical properties of bacterial cell surfaces: An AFM study on Streptococcus mitis strains. Langmuir 19: 2372-2377.

4. Arnoldi M, Kacher CM, Bauerlein E, Radmacher M, Fritz M, 1998. Elastic properties of the cell wall of Magnetospirillum gryphiswaldense investigated by atomic force microscopy. Applied Physics a-Materials Science & Processing 66: S613-S617.

5. Amro NA, Kotra LP, Wadu-Mesthrige K, Bulychev A, Mobashery S, Liu GY, 2000. High-resolution atomic force microscopy studies of the Escherichia coli outer membrane: Structural basis for permeability. Langmuir 16: 2789-2796.

6. Schaer-Zammaretti P, Ubbink J, 2003. Imaging of lactic acid bacteria with AFM - elasticity and adhesion maps and their relationship to biological and structural data. Ultramicroscopy 97: 199-208.

7. Kastowsky M, Gutberlet T, Bradaczek H, 1992. Molecular Modeling of the 3-Dimensional Structure and Conformational Flexibility of Bacterial Lipopolysaccharide. Journal of Bacteriology 174: 4798-4806.

8. Dufrene YF, Boonaert CJP, van der Mei HC, Busscher HJ, Rouxhet PG, 2001. Probing molecular interactions and mechanical properties of microbial cell surfaces by atomic force microscopy. Ultramicroscopy 86: 113-120.

9. Schar-Zammaretti P, Ubbink J, 2003. The cell wall of lactic acid bacteria: Surface constituents and macromolecular conformations. Biophysical Journal 85: 4076-4092.

10. Nataro JP, Steiner T, Guerrant RL, 1998. Enteroaggregative Escherichia coli. Emerging Infectious Diseases 4: 251-261.

11. Sheikh J, Czeczulin JR, Harrington S, Hicks S, Henderson IR, Le Bouguenec C, Gounon P, Phillips A, Nataro JP, 2002. A novel dispersin protein in enteroaggregative Escherichia coli. Journal of Clinical Investigation 110: 1329-1337.

12. Nishi J, Sheikh J, Mizuguchi K, Luisi B, Burland V, Boutin A, Rose DJ,

Blattner FR, Nataro JP, 2003. The export of coat protein from enteroaggregative Escherichia coli by a specific ATP-binding cassette transporter system. Journal of Biological Chemistry 278: 45680-45689.

13. Henderson IR, Hicks S, Navarro-Garcia F, Elias WP, Philips AD, Nataro JP, 1999. Involvement of the enteroaggregative Escherichia coli plasmid-encoded toxin in causing human intestinal damage. Infection and Immunity 67: 5338-5344.

14. Binnig G, Quate CF, Gerber C, 1986. Atomic Force Microscope. Physical Review Letters 56: 930-933.

15. Schaus SS, Henderson ER, 1997. Cell viability and probe-cell membrane interactions of XR1 glial cells imaged by atomic force microscopy. Biophysical Journal 73: 1205-1214.

16. Bottomley LA, Coury JE, First PN, 1996. Scanning probe microscopy. Analytical Chemistry 68: R185-R230.

17. Bolshakova AV, Kiselyova OI, Yaminsky IV, 2004. Microbial surfaces investigated using atomic force microscopy. Biotechnology Progress 20: 1615-1622.

18. Han T, Williams JM, Beebe TP, 1995. Chemical-Bonds Studied with Functionalized Atomic-Force Microscopy Tips. Analytica Chimica Acta 307: 365-376.

19. Allison DP, Hinterdorfer P, Han WH, 2002. Biomolecular force measurements and the atomic force microscope. Current Opinion in Biotechnology 13: 47-51.

20. Arnoldi M, Fritz M, Bauerlein E, Radmacher M, Sackmann E, Boulbitch A, 2000. Bacterial turgor pressure can be measured by atomic force microscopy. Physical Review E 62: 1034-1044.

21. Dufrene YF, 2004. Using nanotechniques to explore microbial surfaces. Nature Reviews Microbiology 2: 451-460.

22. Bhushan B, Koinkar VN, 1994. Nanoindentation Hardness Measurements Using Atomic-Force Microscopy. Applied Physics Letters 64: 1653-1655.

23. Hoh JH, Schoenenberger CA, 1994. Surface-Morphology and Mechanical-Properties of Mdck Monolayers by Atomic-Force Microscopy. Journal of Cell Science 107: 1105-1114.

24. Radmacher M, 1997. Measuring the elastic properties of biological samples with the AFM. IEEE Engineering in Medicine and Biology 16: 47-57.

25. A-Hassan E, Heinz WF, Antonik MD, D'Costa NP, Nageswaran S, Schoenenberger CA, Hoh JH, 1998. Relative microelastic mapping of living cells by atomic force microscopy. Biophysical Journal 74: 1564-1578.

26. Muller DJ, Engel A, 1999. Voltage and pH-induced channel closure of porin OmpF visualized by atomic force microscopy. Journal of Molecular Biology 285: 1347-1351.

27. Walch M, Ziegler U, Groscurth P, 2000. Effect of streptolysin O on the microelasticity of human platelets analyzed by atomic force microscopy. Ultramicroscopy 82: 259-267.

28. Xu W, Mulhern PJ, Blackford BL, Jericho MH, Firtel M, Beveridge TJ, 1996. Modeling and measuring the elastic properties of an archaeal surface, the sheath of Methanospirillum hungatei, and the implication for methane production. Journal of Bacteriology 178: 3106-3112.

29. Touhami A, Nysten B, Dufrene YF, 2003. Nanoscale mapping of the elasticity of microbial cells by atomic force microscopy. Langmuir 19: 4539-4543.

30. Touhami A, Jericho MH, Beveridge TJ, 2004. Atomic force microscopy of cell growth and division in Staphylococcus aureus. Journal of Bacteriology 186: 3286-3295.

31. Vinckier A, Semenza G, 1998. Measuring elasticity of biological materials by atomic force microscopy. FEBS Letters 430: 12-16.

32. Haga H, Sasaki S, Kawabata K, Ito E, Ushiki T, Sambongi T, 2000. Elasticity mapping of living fibroblasts by AFM and immunofluorescence

observation of the cytoskeleton. Ultramicroscopy 82: 253-258.

33. Müller J, 2006. http://www.e-basteln.de/index_o.htm.

34. Sensor Technology Limited, 2006. http://www.sensortech.ca/site/index.cfm?DSP=Page&ID=92.

35. Han WH, Lindsay SM, Jing TW, 1996. A magnetically driven oscillating probe microscope for operation in liquids. Applied Physics Letters 69: 4111-4113.

36. Molecular Imaging Inc., 2006. http://www.molec.com/products_accessories.html#cells.

37. Bolshakova AV, Kiselyova OI, Filonov AS, Frolova OY, Lyubchenko YL, Yaminsky IV, 2001. Comparative studies of bacteria with an atomic force microscopy operating in different modes. Ultramicroscopy 86: 121-128.

38. JPK Instruments, 2006. http://www.lot-oriel.com/site/site_down/nw_force_fren.pdf.

39. Capella B, Baschieri P, Frediani C, Miccoli P, Ascoli C, 1997. Force-distance curves by AFM - A powerful technique for studying surface interactions. Ieee Engineering in Medicine and Biology Magazine 16: 58-65.

40. Domke J, Radmacher M, 1998. Measuring the elastic properties of thin

polymer films with the atomic force microscope. Langmuir 14: 3320-3325.

41. Fang HHP, Chan KY, Xu LC, 2000. Quantification of bacterial adhesion forces using atomic force microscopy (AFM). Journal of Microbiological Methods 40: 89-97.

42. Almqvist N, Delamo Y, Smith BL, Thomson NH, Bartholdson A, Lal R, Brzezinski M, Hansma PK, 2001. Micromechanical and structural properties of a pennate diatom investigated by atomic force microscopy. Journal of Microscopy-Oxford 202: 518-532.

43. Lantz MA, Oshea SJ, Welland ME, 1994. Force Microscopy Imaging in Liquids Using Ac Techniques. Applied Physics Letters 65: 409-411.

44. Li X, Logan BE, 2004. Analysis of bacterial adhesion using a gradient force analysis method and colloid probe atomic force microscopy. Langmuir 20: 8817-8822.

45. Zhdan P, 1997. "In-situ" underwater AFM imaging of the structure of mica. http://www.surrey.ac.uk/MME/Research/SPM/10-1.html.

46. Yu J, Namba Y, 1998. Atomic surface roughness. Applied Physics Letters 73: 3607-3609.

47. Shao ZF, Mou J, Czajkowsky DM, Yang J, Yuan JY, 1996. Biological atomic force microscopy: What is achieved and what is needed. Advances

in Physics 45: 1-86.

48. Camesano TA, Natan MJ, Logan BE, 2000. Observation of changes in bacterial cell morphology using tapping mode atomic force microscopy. Langmuir 16: 4563-4572.

49. Doktycz MJ, Sullivan CJ, Hoyt PR, Pelletier DA, Wu S, Allison DP, 2003. AFM imaging of bacteria in liquid media immobilized on gelatin coated mica surfaces. Ultramicroscopy 97: 209-216.

50. Visai L, Speziale P, Bozzini S, 1990. Binding of Collagens to an Enterotoxigenic Strain of Escherichia-Coli. Infection and Immunity 58: 449-455.

51. Kiernan JA, 1999. Strategies for Preventing Detachment of Sections from Glass Slides. HCWorld Online Information Center for Immunohistochemistry http://www.ihcworld.com/_technical_tips/prevent_section_fall.htm.

52. Sullivan CJ, Morrell JL, Allison DP, Doktycz MJ, 2005. Mounting of *Escherichia coli* spheroplasts for AFM imaging. Ultramicroscopy.

53. Nataro JP, 2005. Personal Communication from Meeting on Collaborative Studies Using AFM to Examine the Surface of Enteroaaggregative *E. Coli*.

54. Burnham NA, Chen X, Hodges CS, Matei GA, Thoreson EJ, Roberts CJ,

Davies MC, Tendler SJB, 2003. Comparison of calibration methods for atomic-force microscopy cantilevers. Nanotechnology 14: 1-6.

55. Cleveland JP, Manne S, Bocek D, Hansma PK, 1993. A Nondestructive Method for Determining the Spring Constant of Cantilevers for Scanning Force Microscopy. Review of Scientific Instruments 64: 403-405.

56. Hutter JL, Bechhoefer J, 1993. Calibration of Atomic-Force Microscope Tips. Review of Scientific Instruments 64: 1868-1873.

57. Dcosta NP, Hoh JH, 1995. Calibration of Optical-Lever Sensitivity for Atomic-Force Microscopy. Review of Scientific Instruments 66: 5096-5097.

58. Velegol SB, Logan BE, 2002. Contributions of bacterial surface polymers, electrostatics, and cell elasticity to the shape of AFM force curves. Langmuir 18: 5256-5262.

59. Bukharaev AA, Mozhanova AA, Nurgazizov NI, Ovchinnikov DV, 2003. Measuring local elastic properties of cell surfaces and soft materials in liquid by atomic force microscopy. Physics of Low-Dimensional Structures 3-4: 31-37.

60. Djabourov M, 1988. Architecture of Gelatin Gels. Contemporary Physics 29: 273-297.

APPENDIX

SUBBING MICA DISCS FOR IMMOBILIZING BACTERIA

A chrome-gelatin adhesive for mounting bacteria on mica substrates was prepared as follows:

0.5g gelatin (sigma G6144)

10 mg chromium ammonium sulfate

100 ml nanopure deionized water at 60 °C

The gelatin was dissolved in 90 ml of heated water. The chromium ammonium sulfate was dissolved in 10 ml water of unheated water. The two solutions were combined at room temperature.

A concentration of 5mg/ml of gelatin corresponds to the minimum concentration for yielding a cross-linked gelatin network (Djabourov, 1988). The chrome gelatin cannot be further diluted with water once cross-linking has occurred, within a few minutes of mixing the components (Kiernan, 1999).

VITA

Melissa A. Beckmann was born in Chicopee Falls, MA. She attended elementary schools in the United Kingdom and several states throughout the United States of America. She graduated from Dickson County High School in Tennessee and then from the University of Tennessee, Knoxville with B.S. and M.S. degrees in Animal Science. She was then accepted to the Genome Science and Technology program with the University of Tennessee and Oak Ridge National Laboratory from which she earned a Master of Science degree in Life Sciences. She is now working at the Mouse Genetics Research Facility at Oak Ridge National Laboratory. She lives in Knoxville and is married to Willie J. Taylor, a food safety scientist.